Better Higgs-*CP* tests through information geometry

Johann Brehmer,[1] Felix Kling,[2] Tilman Plehn,[3] and Tim M. P. Tait[2,4]

[1]*Center for Cosmology and Particle Physics and Center for Data Science, New York, New York 10003, USA*
[2]*Department of Physics and Astronomy, University of California, Irvine, California 92697, USA*
[3]*Institut für Theoretische Physik, Universität Heidelberg, ITP Heidelberg 69120, Germany*
[4]*Institute of Physics and Astronomy, University of Amsterdam, 1098 XH Amsterdam, The Netherlands*

(Received 15 December 2017; published 16 May 2018)

Measuring the *CP* symmetry in the Higgs sector is one of the key tasks of the LHC and a crucial ingredient for precision studies, for example in the language of effective Lagrangians. We systematically analyze which LHC signatures offer dedicated *CP* measurements in the Higgs-gauge sector and discuss the nature of the information they provide. Based on the Fisher information measure, we compare the maximal reach for *CP*-violating effects in weak boson fusion, associated *ZH* production, and Higgs decays into four leptons. We find a subtle balance between more theory-independent approaches and more powerful analysis channels, indicating that rigorous evidence for *CP* violation in the Higgs-gauge sector will likely require a multistep process.

DOI: 10.1103/PhysRevD.97.095017

I. INTRODUCTION

Since the experimental observation of the Higgs boson at the Large Hadron Collider (LHC) [1,2], detailed studies of its properties have become one of the most important laboratories to search for physics beyond the Standard Model. With the measurement of the Higgs mass, the last remaining parameter of the Standard Model has been determined. This implies that further Higgs measurements can be viewed as consistency checks on the validity of the Standard Model description. In particular, deviations from the Standard Model expectations induced by heavy new particles can be described by a continuous and high-dimensional parameter space of Wilson coefficients in the Lagrangian of an effective field theory (EFT) [3–6]. EFT descriptions have the advantage that they are well-defined quantum field theories and allow us to predict and include kinematic distributions in the analysis [7,8].

The key assumptions defining any effective Lagrangian are the particle content and the symmetry structure. Once these two initial assumptions are agreed upon, the Lagrangian is defined as a power series in the heavy new physics scale Λ. First, the general consensus is that the particle content of Higgs analyses is given by the Standard Model particles [9]. However, on the symmetry side, the situation is less clear. To begin with, one can embed the Higgs scalar in a SM-like $SU(2)_L$ doublet or add a scalar field unrelated to the Goldstone modes. In this paper, we realize the electroweak gauge symmetry linearly and include a complex Higgs-Goldstone doublet. A remaining question concerns the charge conjugation (C) and parity (P) symmetries of the Higgs boson and its interactions. In the Standard Model, after the CKM rotations which diagonalize the fermion masses, the Higgs boson has C and P preserving interactions at tree level. Any deviation from this prediction would be a striking manifestation of physics beyond the Standard Model, and it is experimentally exigent to determine whether there are new sources of *CP* violation in the Higgs sector.

A common approach addresses this question by simplistically combining *CP*-even and *CP*-odd operators into one effective Lagrangian and fitting them to a combination of arbitrary observables. Because of the many caveats affecting global dimension-six EFT analyses, the results of such an analysis do not say much about the *CP* nature of the Higgs boson. Instead, we propose to carefully disentangle three questions [10,11]:

(1) Which LHC observables are sensitive to the *CP* nature of the Higgs boson?
(2) What are the assumptions linking these observables to *CP*?
(3) How well can we quantitatively test the Higgs' *CP* properties based on these observables?

Once such a dedicated analysis establishes that *CP* is not a good symmetry of the Higgs sector, we will expand the effective Lagrangian to include *CP*-violating operators to better discern the nature of the *CP* violation. The first two questions have straightforward answers [12]. In fact, there exists a wealth of individual LHC studies for this kind of

measurement in the Higgs-gauge [13–22] and in the Yukawa sectors [23–25], as well as through global analyses [26]. Our focus therefore lies on a unified theory framework which allows us to systematically compare and combine the leading three Higgs-gauge LHC production/decay channels.

Progress on the third question requires the use of modern analysis and tools. The LHC experiments have come to rely on high-level statistical discriminants, including hypothesis tests based on multivariate analysis with machine learning or the matrix element method [27,28]. These tools are able to tease out features that defy simpler cut-and-count analysis based on one-dimensional or two-dimensional kinematic distributions. We apply the new MadFisher approach [29] based on information geometry [30] to systematically study the sensitivity of different Higgs processes to different scenarios of CP violation. Through the Cramér-Rao bound, the Fisher information determines the maximum knowledge about model parameters that can be derived from a given experiment [31]. It allows us to define and to compute the best possible outcome of any multivariate black-box analysis [28,32] as well as the expected outcome based on a more limited set of kinematic observables. In this way, we determine not only which Higgs production and decay processes are best-suited to test its CP properties, but also identify which kinematic variables carry the relevant information.

We begin with a brief review of CP-sensitive observables at the LHC in Sec. I B, CP violation in the Higgs-gauge sector in Sec. I C, and our Fisher information approach in Sec. I D. We study the three leading LHC signatures, Higgs production in weak boson fusion (WBF) in Sec. II, associated ZH production in Sec. III, and Higgs decays to four leptons in Sec. IV. For each of these signatures we discuss the possible CP-sensitive observables and briefly describe the advantages and challenges of the corresponding LHC analysis. In Sec. V, we compare all three channels.

A. CP vs naive time reversal

As is well known, the three discrete symmetries consistent with Lorentz invariance and a Hamiltonian which is Hermitian [12] are charge conjugation (C), parity (P), and time reversal (T). These three operators act on a complex scalar field $\phi(t,\vec{x})$ as

$$\begin{aligned} C\phi(t,\vec{x})C^{-1} &= \eta_C\phi^*(t,\vec{x}) \\ P\phi(t,\vec{x})P^{-1} &= \eta_P\phi(t,-\vec{x}) \\ T\phi(t,\vec{x})T^{-1} &= \eta_T\phi(-t,\vec{x}), \end{aligned} \tag{1}$$

where the phases η_j define the intrinsic symmetry properties of ϕ. C and P are unitary transformations, while T is antiunitary, implying that the phase η_T is not measurable and can be chosen to be $\eta_T = 1$. Acting on a single-particle state with 4-momentum p and spin s produces

$$\begin{aligned} C|\phi(p,s)\rangle &= |\phi^*(p,s)\rangle \\ P|\phi(p,s)\rangle &= \eta_\phi|\phi(-p,s)\rangle \\ T|\phi(p,s)\rangle &= \langle\phi(-p,-s)|, \end{aligned} \tag{2}$$

where η_ϕ is the intrinsic parity of the field. Time reversal transforms incoming states into outgoing states, so it is convenient to define a "naive time reversal" [10,12,33],

$$\hat{T}|\phi(p,s)\rangle = |\phi(-p,-s)\rangle, \tag{3}$$

which explicitly omits exchanging initial and final states.

Observables can be chosen to reflect the C, P, or T transformation properties of the underlying transition amplitude. We are interested in a real-valued observable O that can be measured in a process $|i\rangle \to |f\rangle$. Interesting observables at the LHC are functions of the 4-momenta, spins, flavors, and charges of initial and final states. First, we define a U-odd or U-even observable as

$$O(U|i\rangle \to U|f\rangle) = \mp\, O(|i\rangle \to |f\rangle) \quad \text{for } U = C, P, \hat{T}, \tag{4}$$

where the upper (lower) sign refers to U-odd (U-even).

For the purpose of testing the properties of the underlying theory, a *genuine* U-odd observable is defined as having a vanishing expectation value in a U-symmetric theory (for which $\mathcal{L} = U\mathcal{L}U^{-1}$),

$$\langle O\rangle_{\mathcal{L}=U\mathcal{L}U^{-1}} = 0. \tag{5}$$

In case the initial state is a U eigenstate, or the probability distribution of the initial states $p(|i\rangle)$ is U-symmetric, the second definition is slightly weaker. One can show that, under this condition, any U-odd observable is also genuinely U-odd,

$$\begin{aligned} &O(U|i\rangle \to U|f\rangle) = -O(|i\rangle \to |f\rangle) \quad \text{(odd)} \\ &\xrightarrow{p(|i\rangle)=p(U|i\rangle)} \langle O\rangle_{\mathcal{L}=U\mathcal{L}U^{-1}} = 0 \quad \text{(genuine odd)}. \end{aligned} \tag{6}$$

In particular, any observable that compares the probabilities of two conjugated processes,

$$O \propto \mathrm{d}\sigma(|i\rangle \to |f\rangle) - \mathrm{d}\sigma(U|i\rangle \to U|f\rangle), \tag{7}$$

is obviously genuinely U-odd.

We can gain additional insights on CP from the $\hat{T}$ transformation properties. Based on the definition in Eq. (5), at tree level, a finite expectation value of a genuine $\hat{T}$-odd observable O indicates a CP-violating theory [34]. In addition to CPT invariance, this argument requires

(i) the phase space is $\hat{T}$-symmetric;
(ii) the initial state is a $\hat{T}$-eigenstate, or its distribution is invariant under $\hat{T}$; and
(iii) there cannot be rescattering effects.

The latter correspond to absorptive, complex-valued loop contributions, for instance an imaginary part in the propagator of an intermediate on-shell particle. To illustrate this point, consider the transition amplitude $\mathcal{T}$ defined via $S = 1 + i\mathcal{T}$. The matrix elements satisfy

$$\langle f|\mathcal{T}|i\rangle \overset{CP\text{-invariant}}{=} \langle i_T|\mathcal{T}|f_T\rangle \overset{\text{no re-scattering}}{=} \langle f_T|\mathcal{T}|i_T\rangle^* \Rightarrow |\langle f|\mathcal{T}|i\rangle|^2 = |\langle f_T|\mathcal{T}|i_T\rangle|^2, \tag{8}$$

with $T|i\rangle = \langle i_T|$ as given in Eq. (2), etc. The first step follows from CPT invariance, and the second from the optical theorem in the absence of rescattering. Indeed, in a CP-symmetric theory and in the absence of rescattering, the matrix element squared is $\hat{T}$-invariant.

In practice, this argument means that where genuine CP observables cannot be constructed, we can analyze genuine $\hat{T}$ observables instead. A nonzero expectation value here is evidence for CP violation under the additional assumption of no or negligible rescattering.

B. *CP* violation in LHC processes

We evaluate the effect of CP-odd operators on the three most promising LHC Higgs signatures: WBF Higgs production in Sec. II, associated ZH production in Sec. III, and Higgs decays to four leptons in Sec. IV. From Fig. 1, it is clear that these three processes are governed by the same hard process, with different initial and final state assignments, and the W and Z couplings related by custodial symmetry [15,22,35].

Since it is not realistically possible to determine the spins in the initial or final states in these processes, all observables must be constructed as functions of the 4-momenta. Ideally, we can reconstruct four independent external 4-momenta for each process shown in Fig. 1 and combine them into ten scalar products of the type $(p_i \cdot p_j)$. Four of them correspond to the masses of the initial- and final-state particles, and the remaining six specify the kinematics. Scalar products are P-even. Equation (3) implies that they transform the same way under $\hat{T}$ as under P, so they are also $\hat{T}$-even. As we will see in Sec. II A, two of them are C-odd, while the remaining four are C-even. In addition to the scalar products, there is one P-odd and $\hat{T}$-odd observable constructed from four independent 4-momenta, $\epsilon_{\mu\nu\rho\sigma} k_1^\mu k_2^\nu q_1^\rho q_2^\sigma$ [15,16]. Altogether, there are

(i) four scalar products corresponding to masses of the external particles;
(ii) four C-even, P-even, and $\hat{T}$-even scalar products;
(iii) two C-odd, P-even, and $\hat{T}$-even scalar products;
(iv) one C-even, P-odd, and $\hat{T}$-odd observable constructed from the Levi-Civita-tensor,

for all three processes illustrated in Fig. 1. More details, including some analytic results, are given in the Appendix. Thus, at most, three observables are CP-odd, with the main difference between each process coming from what can be measured for each of the four fermion lines.

In cases where the initial state is guaranteed to be CP-even and $\hat{T}$-even, or can be boosted into such a frame, we can distinguish two types of CP-odd observables:

(1) CP-odd and $\hat{T}$-odd: for the $q\bar{q}$ initial state this implies that the observable is also genuine CP-odd and genuine $\hat{T}$-odd [see Eq. (6)]. In a CP-symmetric theory its expectation value vanishes, implying that a nonzero expectation value requires CP violation regardless of the presence of rescattering. The different cases are illustrate in the upper half of Table I.
(2) CP-odd and $\hat{T}$-even: for the $q\bar{q}$ initial state the observable is also genuine CP-odd, so in a CP-symmetric theory its expectation value vanishes. In the lower half of Table I we show the different scenarios: if the theory is CP-violating, the corresponding expectation values does not vanish. If we ignore rescattering, the theory also appears $\hat{T}$-violating, but the expectation value of the $\hat{T}$-even observable combined with an antisymmetric amplitude will still vanish. However, in the presence of rescattering or another complex phase, this unwanted condition from the $\hat{T}$ symmetry vanishes, and the expectation for $\langle O\rangle$ matches the symmetry of the theory.

This implies that for a (statistically) CP-symmetric initial state, one can arrive at a meaningful statement about the CP symmetry of the underlying theory either through a CP-odd and $\hat{T}$-odd observable without any assumption about complex phases or through a CP-odd and $\hat{T}$-even observable in the presence of a complex phase.

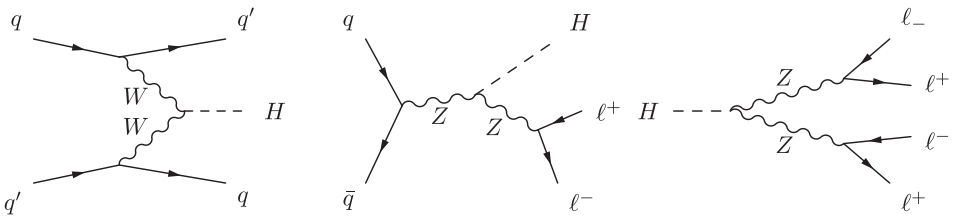

FIG. 1. Feynman diagrams describing the three processes considered in this paper: WBF Higgs production, associated ZH production, and $H \to 4\ell$ decays.

TABLE I. Predictions for CP-odd observables O based on the theory's symmetries and the observable's transformation properties under $\hat{T}$. In all cases we assume that the initial state or its probability distribution is symmetric under both CP and $\hat{T}$.

Observable	Theory	Rescattering	Symmetry argument		Prediction
CP-odd, $\hat{T}$-odd	CP-symmetric	No	CP and $\hat{T}$: symmetric σ_{int}, odd O	$\Rightarrow$	$\langle O\rangle = 0$
		Yes	CP: symmetric σ_{int}, odd O	$\Rightarrow$	$\langle O\rangle = 0$
	CP-violating	No			Can have $\langle O\rangle \neq 0$
		Yes			Can have $\langle O\rangle \neq 0$
CP-odd, $\hat{T}$-even	CP-symmetric	No	CP: symmetric σ_{int}, odd O	$\Rightarrow$	$\langle O\rangle = 0$
		Yes	CP: symmetric σ_{int}, odd O	$\Rightarrow$	$\langle O\rangle = 0$
	CP-violating	No	$\hat{T}$: antisymmetric σ_{int}, even O	$\Rightarrow$	$\langle O\rangle = 0$
		Yes			Can have $\langle O\rangle \neq 0$

C. *CP* violation in the Higgs-gauge sector

Typical tests of C, P, or T symmetries of the Higgs sector do not probe the symmetry nature of the actual Higgs field, but rather the transformation properties of the action through its influence on S-matrix elements. We focus on the transformation properties of observables and explore how they reflect the symmetry structure of the Higgs Lagrangian. To this end, we evaluate the effect of CP-violating as opposed to CP-conserving Higgs couplings to weak bosons or heavy fermions. For an effective Higgs-gauge Lagrangian truncated at mass dimension six,

$$\mathcal{L} = \mathcal{L}_{\text{SM}} + \frac{f_i}{\Lambda^2}\mathcal{O}_i, \tag{9}$$

our CP-even reference scenario consists of the renormalizable Standard Model Lagrangian combined with the five CP-even dimension-six operators in the HISZ basis [6,7,36],

$$\begin{aligned}
\mathcal{O}_B &= i\frac{g}{2}(D^\mu\phi^\dagger)(D^\nu\phi)B_{\mu\nu}\\
\mathcal{O}_W &= i\frac{g}{2}(D^\mu\phi)^\dagger\sigma^k(D^\nu\phi)W^k_{\mu\nu}\\
\mathcal{O}_{BB} &= -\frac{g'^2}{4}(\phi^\dagger\phi)B_{\mu\nu}B^{\mu\nu}\\
\mathcal{O}_{WW} &= -\frac{g^2}{4}(\phi^\dagger\phi)W^k_{\mu\nu}W^{\mu\nu k}\\
\mathcal{O}_{\phi,2} &= \frac{1}{2}\partial^\mu(\phi^\dagger\phi)\partial_\mu(\phi^\dagger\phi).
\end{aligned} \tag{10}$$

At the same mass dimension, CP-odd couplings are described by the operators

$$\begin{aligned}
\mathcal{O}_{B\tilde{B}} &= -\frac{g'^2}{4}(\phi^\dagger\phi)\tilde{B}_{\mu\nu}B^{\mu\nu} \equiv -\frac{g'^2}{4}(\phi^\dagger\phi)\epsilon_{\mu\nu\rho\sigma}B^{\rho\sigma}B^{\mu\nu}\\
\mathcal{O}_{W\tilde{W}} &= -\frac{g^2}{4}(\phi^\dagger\phi)\tilde{W}^k_{\mu\nu}W^{\mu\nu k} \equiv -\frac{g^2}{4}(\phi^\dagger\phi)\epsilon_{\mu\nu\rho\sigma}W^{\rho\sigma k}W^{\mu\nu k}.
\end{aligned} \tag{11}$$

With the Levi-Civita tensor, these operators break down as C-conserving and P-violating. Field redefinitions provide the freedom to exchange certain dimension-six operators for others according to the equations of motions without affecting the S-matrix elements. However, these CP-odd operators do not appear in the relevant equations of motions, so they are not affected by this basis choice [37].

While the effective Lagrangians in Eqs. (10) and (11) demand real coefficients f_{WW} and $f_{W\tilde{W}}$, it is also interesting to observe what happens when they are taken to be complex. Strictly speaking, this does not occur in an EFT from integrating out massive degrees of freedom in a well-defined UV theory. However, absorptive complex phases can appear through light degrees of freedom, even in the Standard Model, for instance from electroweak corrections or in Higgs production with a hard jet [38,39]. An explicit example showing how an absorptive complex phase appears in the Higgs-gluon coupling can be found in Appendix A of Ref. [40]. Such loop-induced contributions to the expectation value of CP-odd observables must be taken into account in precision measurements. These cases are not technically described by a local EFT and could lead to different momentum dependences, and we leave a more refined treatment of this case for future work. Instead, we consider coefficients such as f_{WW} and $f_{W\tilde{W}}$ to be complex to demonstrate how such cases complicate the determination of the CP nature of the Higgs interactions. We emphasize that we use these imaginary parts of Wilson coefficients only as a simple toy model to illustrate under what circumstances CP-even physics could mimic CP-odd signatures in the context of this study, not as a valid part of an effective operator analysis. This caveat includes the fact that they are not process-independent properties of an underlying Lagrangian and should not be considered as part of any global Higgs analysis.

Combining the different pieces, we arrive at 13 model parameters of interest,

$$\begin{aligned}
\mathbf{g} = \frac{v^2}{\Lambda^2}(&f_{\phi,2}\, f_W f_B f_{WW} f_{BB} f_{W\tilde{W}} f_{B\tilde{B}}\,\text{Im}f_W\,\text{Im}f_B\\
&\times \text{Im}f_{WW}\,\text{Im}f_{BB}\,\text{Im}f_{W\tilde{W}}\,\text{Im}f_{B\tilde{B}})^T,
\end{aligned} \tag{12}$$

where the factor v^2 ensures that the model parameters are dimensionless. The first seven entries represent the usual

Wilson coefficients in the EFT. The last six entries allow for a toy model of absorptive contributions. We will use this full vector of model parameters to analyze the sensitivity of different processes to the *CP* properties of the Higgs-gauge sector.

D. Information geometry and Cramér-Rao bound

We briefly review the basics of information geometry applied to Higgs physics at the LHC, as introduced in Ref. [29]. The LHC measurements are represented by a set of events with kinematic observables $\mathbf{x}$. Their distribution depends on a vector of model parameters, for example Higgs couplings, with unknown true values $\mathbf{g}$. An analysis leads to an estimator $\hat{\mathbf{g}}$, designed to follow a probability distribution around the true values. For an unbiased estimator the corresponding expectation values are equal to the true values, $\bar{g}_i \equiv E[\hat{g}_i|\mathbf{g}] = g_i$. The typical error of the measurement is described by the covariance matrix,

$$C_{ij}(\mathbf{g}) \equiv E[(\hat{g}_i - \bar{g}_i)(\hat{g}_j - \bar{g}_j)|\mathbf{g}], \tag{13}$$

which, as a generalization of the variance in one dimension, gives the precision of the measurement: the smaller C_{ij}, the better one can measure the combination of couplings g_i and g_j.

The second object of interest is the Fisher information matrix, the first term in a Taylor series of the log-likelihood around its maximum, which measures the sensitivity of the likelihood of experimental outcomes $\mathbf{x}$ to the model parameters $\mathbf{g}$. The Fisher information matrix can be computed from the probability distribution $f(\mathbf{x}|\mathbf{g})$ for a specific phase space configuration given a model, as

$$I_{ij}(\mathbf{g}) \equiv -E\left[\frac{\partial^2 \log f(\mathbf{x}|\mathbf{g})}{\partial g_i \partial g_j}\middle|\mathbf{g}\right]. \tag{14}$$

A large entry in the Fisher matrix implies that the measurement is particularly sensitive to a given model parameter combination $g_{i,j}$. Conversely, an eigenvector of the Fisher matrix with zero eigenvalue indicates a blind direction, corresponding to a combination of measurements with no expected impact.

The Cramér-Rao bound [31] links these two tracers of the sensitivity of a measurement: the (inverse) Fisher information tells us how much information a given experiment can optimally extract about a set of model parameters. The covariance matrix gives the actual uncertainty of the measurements, and its minimum value must be larger than the inverse Fisher information,

$$C_{ij}(\mathbf{g}) \geq (I^{-1})_{ij}(\mathbf{g}). \tag{15}$$

The Fisher information is invariant under a reparametrization of the observables $\mathbf{x}$, and transforms covariantly under a reparametrization of the model parameters $\mathbf{g}$. After removing blind directions, the Fisher information is a symmetric and positive definite rank-two tensor and defines a metric on the model space [30]. The model-space distance measure,

$$d(\mathbf{g}_b; \mathbf{g}_a) = \sqrt{(\mathbf{g}_a - \mathbf{g}_b)_i I_{ij}(\mathbf{g}_a)(\mathbf{g}_a - \mathbf{g}_b)_j}, \tag{16}$$

gives contours of constant distances as optimal error ellipsoids. Strictly speaking, it is defined in the tangent space at $\mathbf{g}_a$, but can easily be extended to distances calculated along geodesics on the theory manifold [29]. Such local or global distances track how (un)likely it is to measure $\hat{\mathbf{g}} = \mathbf{g}_b$ given $\mathbf{g} = \mathbf{g}_a$. In the Gaussian limit, the distance value is measured in standard deviations.

The distributions $f(\mathbf{x}|\mathbf{g})$ entering Eq. (14) can be computed for any model from Monte-Carlo simulations combined with a detector simulation. The corresponding measurement consists of an observed n events distributed over phase space positions $\mathbf{x}$. For a total cross section $\sigma(\mathbf{g})$ and an integrated luminosity L the full probability distribution in Eq. (14) factorizes [28,32] as

$$f(\mathbf{x}_1, \ldots, \mathbf{x}_n|\mathbf{g}) = \text{Pois}(n|L\sigma(\mathbf{g})) \prod_{i=1}^{n} f^{(1)}(\mathbf{x}_i|\mathbf{g}), \tag{17}$$

where $f^{(1)}(\mathbf{x}|\mathbf{g})$ is the normalized probability distribution for a single event populating $\mathbf{x}$ and can be computed by standard event generators. The factorized Fisher information is

$$I_{ij} = \frac{L}{\sigma}\frac{\partial\sigma}{\partial g_i}\frac{\partial\sigma}{\partial g_j} - L\sigma E\left[\frac{\partial^2 \log f^{(1)}(\mathbf{x}|\mathbf{g})}{\partial g_i \partial g_j}\right]. \tag{18}$$

This total Fisher information can be calculated from Monte-Carlo simulations. It defines the best possible precision with which the parameters $\mathbf{g}$ can be measured based on the full observable space, independent of the (multivariate) analysis strategy. It also intrinsically includes all directions in theory space and all correlations between different parameters and does not require any discretization of the parameter space.

Given the discussion in Sec. I B, an interesting question is how much of the full information is included in particular kinematic distributions. To answer it, we alternatively calculate the information in one-dimensional or two-dimensional histograms of kinematic observables. This gives the maximum precision with which parameters can be measured by analyzing a given set of observables. Comparing this reduced Fisher information to the total information based on the full phase space lets us quantitatively analyze whether the clearer theory interpretation of well-defined *CP* observables is worth the loss in sensitivity compared to a multivariate approach.

We evaluate the resulting Fisher information matrices in three ways. First, we calculate curves of constant distances given by Eq. (16) in the space of dimension-six Wilson coefficients, corresponding to optimal expected exclusion limits of an analysis. This allows us to study correlations between different Wilson coefficients, for example between *CP*-violating and *CP*-conserving operators.

Second, we can rotate the symmetric Fisher information matrix I_{ij} into its diagonal form, defining eigenvectors as a superposition of model parameters and the corresponding information eigenvalue. In the diagonal form, the Cramér-Rao bound conveniently defines the reach of a given analysis in each eigenvector direction. Numerically, this reach can be expressed in terms of the Wilson coefficients $\Lambda/\sqrt{f}$, as defined in Eq. (9) [29]. We discuss this analysis in terms of model-space eigenvectors and their reach in Sec. V.

Finally, if we are especially interested in a subset of parameters, we can compute the corresponding Fisher information either setting all operators to zero, or by profiling over all other operators, as discussed in detail in the Appendix of Ref. [29]. In Sec. V, we use this procedure to analyze the robustness of signatures from *CP*-violating operators to other scenarios of new physics.

II. HIGGS PRODUCTION IN WEAK BOSON FUSION

To construct appropriate kinematic observables for WBF Higgs production, we can in principle make use of three final-state momenta and two initial-state momenta, where one momentum is linearly dependent on the other four due to energy-momentum conservation. We assume the Higgs decay $H \to \tau\tau$, which allows us to approximately reconstruct the Higgs 4-momentum [41], though this specific choice of decay mode is expected to have little if any impact on the final results [15]. Throughout the discussion, we rely on the reconstruction of the Higgs momentum to reconstruct the missing information about the initial parton momenta.

A. *CP* observables

The partonic qq' initial state of weak boson fusion is not a C eigenstate. The discussion in Sec. I B thus implies that one cannot construct a production-side genuine *CP*-sensitive observable in WBF Higgs production. On the other hand, Eq. (3) states that in the absence of spin information the transformation properties under P and $\hat{T}$ are the same, and thus one can construct exactly one genuine $\hat{T}$-odd observable based on the Levi-Civita tensor in the center-of-mass frame, making use of the fact that the initial state probability distribution is $\hat{T}$-symmetric in proton-proton collisions. In the absence of large rescattering effects, it probes *CP* violation in the Higgs-gauge sector. This observable can be naively defined as [15,16]

$$\epsilon_{\mu\nu\rho\sigma} k_1^\mu k_2^\nu q_1^\rho q_2^\sigma, \tag{19}$$

where the two incoming parton momenta are $k_{1,2}$ and the two outgoing tagging jet momenta are $q_{1,2}$. However, this definition suffers from the feature that it changes sign under exchange of the two tagging jet momenta $q_1 \leftrightarrow q_2$. We remove this ambiguity through the modification [10]

$$O \equiv \epsilon_{\mu\nu\rho\sigma} k_1^\mu k_2^\nu q_1^\rho q_2^\sigma \,\mathrm{sign}[(k_1 - k_2)\cdot(q_1 - q_2)]. \tag{20}$$

Defining k_+ and k_- to be the initial state momenta in the lab frame pointing along the positive and negative beam axis (z direction), q_+ and q_- are delineated "forward" and "backward" such that k_+ and q_+ point to the same hemisphere, or more generally $(q_+ - q_-)\cdot(k_+ - k_-) > 0$ [16]. This implies that $(q_+)_z > (q_-)_z$ in the center-of-mass frame. In this notation,

$$O = \epsilon_{\mu\nu\rho\sigma} k_+^\mu k_-^\nu q_+^\rho q_-^\sigma. \tag{21}$$

In the laboratory frame, $k_\pm = (E_\pm, 0, 0, \pm E_\pm)$. The assignment for $q_\pm$ implies that the sign factor is always unity, which reduces O to a triple product,

$$O = 2E_+E_-(q_{y,+}q_{x,-} - q_{x,+}q_{y,-}) = 2E_-(\vec{q}_- \times \vec{q}_+)\cdot\vec{k}_+, \tag{22}$$

or, in terms of $q_{x,\pm} = q_{T,\pm}\cos\phi_\pm$ and $q_{y,\pm} = q_{T,\pm}\sin\phi_\pm$,

$$O = 2E_+E_-q_{T,+}q_{T,-}\sin\Delta\phi_{jj}, \tag{23}$$

where $\Delta\phi_{jj}$ is the signed azimuthal angle difference,

$$\Delta\phi_{jj} \equiv \phi_+ - \phi_-. \tag{24}$$

The main weakness in the observable O is that it depends on the (usually) poorly determined energies of the initial state partons $E_\pm$. Rather than relying on the reconstruction of the Higgs momentum via its decay products to provide this information, we replace the full observable by

$$O \to \Delta\phi_{jj}, \tag{25}$$

which retains the *CP* sensitivity through the well-defined $\hat{T}$ transformation of the full set of observable, matrix element, and initial state. The primary difference between the Lorentz-invariant observable O and $\Delta\phi_{jj}$ is that O is more sensitive to the magnitude of the tagging jet momenta. This can be advantageous in some instances, since the dimension-six operators in the EFT lead to modifications which grow with momentum transfer. However, the same effect can be achieved by supplementing $\Delta\phi_{jj}$ with a virtuality measure such as the transverse momentum of the harder jet.

We simulate the WBF process with the MadMax [42,43] setup of MadGraph [44]. We compute the $\Delta\phi_{jj}$ distribution (with the same event selection as described below) predicted by the Standard Model as well as for the Standard Model augmented by representative operators $\mathcal{O}_{WW}$ and $\mathcal{O}_{W\tilde{W}}$ defined in Eqs. (10) and (11). The resulting distributions are shown in Fig. 2. As expected, the Standard Model, even when supplemented by a *CP*-even operator such as f_{WW}, results in a distribution that is symmetric under $\Delta\phi_{jj} \to -\Delta\phi_{jj}$. The interference term with the Standard Model is largest for $\Delta\phi_{jj} = 0, \pm\pi$, similar to the dimension-six squared contribution [15]. In contrast, the interference of

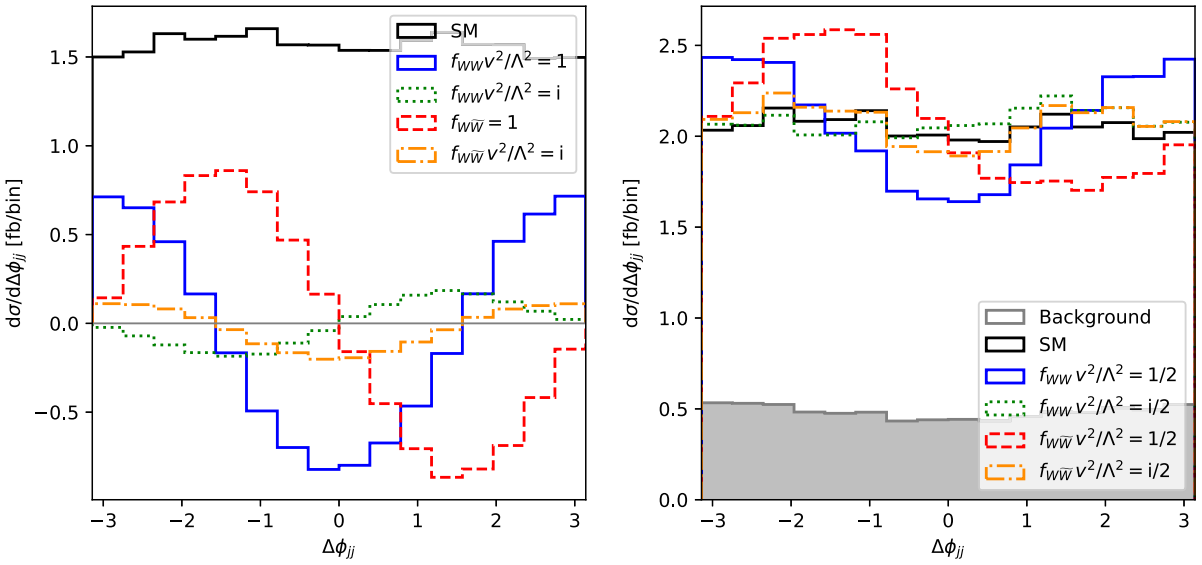

FIG. 2. Distribution of the signed angle $\Delta\phi_{jj}$ in WBF Higgs production after the cuts in Eqs. (27) and (29) for the Standard Model (black) as well as the for the EFT with the indicated Wilson coefficients. In the left panel we show the SM signal (black) as well as the interference of different dimension-six amplitudes with the SM signal (colored). The right panel shows the full distributions including the backgrounds (grey).

the *CP*-odd operator with the Standard Model is antisymmetric under $\Delta\phi_{jj} \to -\Delta\phi_{jj}$. It vanishes in the case where the external momenta are no longer linearly independent, namely $|\Delta\phi_{jj}| = 0, \pi$ [15]. Similar results would be obtained for the other *CP*-even operators of Eq. (10) such as $\mathcal{O}_W$. In contrast, the *CP*-odd operator $\mathcal{O}_{W\tilde{W}}$ leads to a distribution with a clear preference for $\Delta\phi_{jj} < 0$.

As is evident from Fig. 2, an imaginary Wilson coefficient f_{WW} also leads to an asymmetry in the $\Delta\phi_{jj}$ distribution. Clearly, absorptive phases can mimic the signatures from *CP*-violating scenarios in this nongenuine *CP* observable, and thus potentially complicate the interpretation of such a signature.

B. LHC reach

Based on our simulations, we determine the expected LHC sensitivity to $\mathcal{O}_{W\tilde{W}}$ through WBF production followed by the $H \to \tau\tau$ decay. The dominant backgrounds are QCD and electroweak Zjj production followed by the decay $Z \to \tau\tau$, and Higgs production in gluon fusion with $H \to \tau\tau$. Our analysis is based on the tagging jet kinematics [45–47]. We simulate the WBF signal following Ref. [29] by generating the process

$$pp \to Hjj \to \tau^+\tau^- jj, \tag{26}$$

multiplying the rates with the branching ratio for the semileptonic di-tau mode, and assuming the di-tau system to be reconstructed with a realistic resolution for $m_{\tau\tau}$. This means that as the leading detector effect the $m_{\tau\tau}$ distribution is smeared by a Gaussian [32,42,43] (with width 17 GeV) for Higgs production and a double Gaussian (where the dominant component has a width of 13 GeV) for Z production, as estimated from Fig. 1(a) of Ref. [48]. The double Gaussian ensures an accurate description of the high-mass tail of the Z peak around $m_{\tau\tau} = m_H$ [49].

Event selection proceeds first with loose cuts,

$$\begin{aligned} p_{T,j} &> 20\ \text{GeV} \qquad |\eta_j| < 5.0 \qquad \Delta\eta_{jj} > 2.0 \\ p_{T,\tau} &> 10\ \text{GeV} \qquad |\eta_\tau| < 2.5, \end{aligned} \tag{27}$$

to retain as much phase space information as possible. One can improve discrimination of the WBF signal from the electroweak and QCD background processes based on their different radiation patterns [45]. These selections are simulated by applying central jet veto (CJV) survival probabilities [41],

$$\begin{aligned} \varepsilon^{\text{CJV}}_{\text{WBF}\,H} &= 0.71 \qquad \varepsilon^{\text{CJV}}_{\text{EW}\,Z} = 0.48 \\ \varepsilon^{\text{CJV}}_{\text{QCD}\,Z} &= 0.14 \qquad \varepsilon^{\text{CJV}}_{\text{GF}\,H} = 0.14. \end{aligned} \tag{28}$$

Provided the hard phase space does not include any jets beyond the two tagging jets, the results are not expected to first approximation to be sensitive to details of the central jet veto. For simplicity, we assume the reconstruction and identification of the leptonic τ to be fully efficient and assume a constant overall efficiency of 0.6 for the hadronic tau. These efficiencies do not affect the signal-to-background ratio. As a second way to suppress backgrounds, we apply a likelihood-based event selection [29],

$$\frac{\Delta\sigma_{\text{SM WBF}}(\mathbf{x})}{\Delta\sigma_{\text{backgrounds}}(\mathbf{x})} > 1, \tag{29}$$

retaining only phase-space points $\mathbf{x}$ with an expected signal-to-background ratio of at least unity.

For an integrated luminosity of $L = 100\ \text{fb}^{-1}$, after all efficiencies and the event selection of Eqs. (27) and (29), we expect a WBF Higgs signal of 1349 events in the Standard Model, together with a total expected background of 388 events. It is worth noting that these numbers are optimistic and do not include the full suite of detector effects, fake backgrounds, etc.

We analyze how well WBF production can extract information about CP violation in the dimension-six EFT defined in Eqs. (10) and (11). The model parameters of interest are given in Eq. (12). For these directions in the EFT parameter space, we use the MadFisher tools [29] to find the Fisher information evaluated at the Standard Model after $L = 100\ \text{fb}^{-1}$ to be

$$I_{ij} = \begin{array}{c} \begin{matrix} f_{\phi,2} & f_W & f_B & f_{WW} & f_{BB} & f_{W\widetilde{W}} & f_{B\tilde{B}} & \text{Im}\, f_W & \text{Im}\, f_B & \text{Im}\, f_{WW} & \text{Im}\, f_{BB} & \text{Im}\, f_{W\widetilde{W}} & \text{Im}\, f_{B\tilde{B}} \end{matrix} \\ \begin{pmatrix} 4942 & -968 & -50 & 54 & 2 & -7 & 0 & -1 & 0 & 2 & 0 & 36 & 0 \\ -968 & 715 & 35 & -191 & -3 & 1 & 0 & 0 & 0 & 0 & 0 & -55 & -1 \\ -50 & 35 & 6 & -9 & 0 & 0 & 0 & 0 & 0 & 0 & 0 & -2 & 0 \\ 54 & -191 & -9 & 321 & 3 & -1 & 0 & 0 & 0 & 1 & 0 & 72 & 1 \\ 2 & -3 & 0 & 3 & 0 & 0 & 0 & 0 & 0 & 0 & 0 & 1 & 0 \\ -7 & 1 & 0 & -1 & 0 & 359 & 4 & 41 & 1 & -81 & -1 & -1 & 0 \\ 0 & 0 & 0 & 0 & 0 & 4 & 0 & 0 & 0 & -1 & 0 & 0 & 0 \\ -1 & 0 & 0 & 0 & 0 & 41 & 0 & 6 & 0 & -12 & 0 & 0 & 0 \\ 0 & 0 & 0 & 0 & 0 & 1 & 0 & 0 & 0 & 0 & 0 & 0 & 0 \\ 2 & 0 & 0 & 1 & 0 & -81 & -1 & -12 & 0 & 23 & 0 & 0 & 0 \\ 0 & 0 & 0 & 0 & 0 & -1 & 0 & 0 & 0 & 0 & 0 & 0 & 0 \\ 36 & -55 & -2 & 72 & 1 & -1 & 0 & 0 & 0 & 0 & 0 & 21 & 0 \\ 0 & -1 & 0 & 1 & 0 & 0 & 0 & 0 & 0 & 0 & 0 & 0 & 0 \end{pmatrix} \end{array} \begin{matrix} f_{\phi,2} \\ f_W \\ f_B \\ f_{WW} \\ f_{BB} \\ f_{W\widetilde{W}} \\ f_{B\tilde{B}} \\ \text{Im}\, f_W \\ \text{Im}\, f_B \\ \text{Im}\, f_{WW} \\ \text{Im}\, f_{BB} \\ \text{Im}\, f_{W\widetilde{W}} \\ \text{Im}\, f_{B\tilde{B}} \end{matrix}, \tag{30}$$

where red entries correspond to the CP-odd coefficients and we explicitly label the rows and columns with the corresponding Wilson coefficients. Note that the Fisher information on the real parts of the Wilson coefficients is independent of the Fisher information on the imaginary components and thus on our toy model of absorptive physics.

Figure 3 shows the corresponding optimal error contours for representative pairs of Wilson coefficients, with those not shown on the axes set to zero, assuming that the data follow the Standard Model expectation. We assume the cuts of Eqs. (27) and (29) and an integrated luminosity of $100\ \text{fb}^{-1}$. Since these two-dimensional combinations of Wilson coefficients may not correspond to realistic UV scenarios, the projections should be interpreted with care.

In addition to the full phase-space information, which obviously results in the best reach, we show the expected constraints from observables based on subsets of the information contained in the $\Delta\phi_{jj}$ distribution. First, we find that all of the observables are sensitive to various CP-even operators. Second, the signed $\Delta\phi_{jj}$ distribution contains approximately as much information about $\mathcal{O}_{WW}$ as about $\mathcal{O}_{W\tilde{W}}$. In contrast, the distribution of its absolute value $|\Delta\phi_{jj}|$ is only sensitive to the CP-even operators. In Fig. 3 we confirm that in the top-left panel the full $\Delta\phi_{jj}$ results are identical to those from the absolute value $|\Delta\phi_{jj}|$, while in the two bottom panels with their imaginary parts they are identical to those from the asymmetry,

$$a_{\Delta\phi_{jj}} \equiv \frac{d\sigma(\Delta\phi_{jj}) - d\sigma(-\Delta\phi_{jj})}{d\sigma(\Delta\phi_{jj}) + d\sigma(-\Delta\phi_{jj})}. \tag{31}$$

By definition, this asymmetry is not sensitive to CP-even modification with a real Wilson coefficient. This confirms that any asymmetry in $\Delta\phi_{jj}$ is a clear indicator of CP violation as long as we neglect absorptive phases.

The observable O is insensitive to the CP-even operator $\mathcal{O}_{WW}$, because the information in the absolute value $|\Delta\phi|$ is washed out by the residual momentum dependence. The same momentum dependence, on the other hand, results in a slightly enhanced reach for CP-violating physics compared to $a_{\Delta\phi_{jj}}$. This is consistent with the observation that supplementing $\Delta\phi_{jj}$ with the leading $p_{T,j}$ and analyzing their joint distribution also significantly improves the reach. This enhancement is not *per se* related to CP violation, but rather reflects the well known fact that dimension-six operators lead to effects which are enhanced at higher momentum transfer. These two important distributions cover the majority of the information after the selection cuts in Eqs. (27) and (29), with only modest improvements obtained by including additional phase-space information.

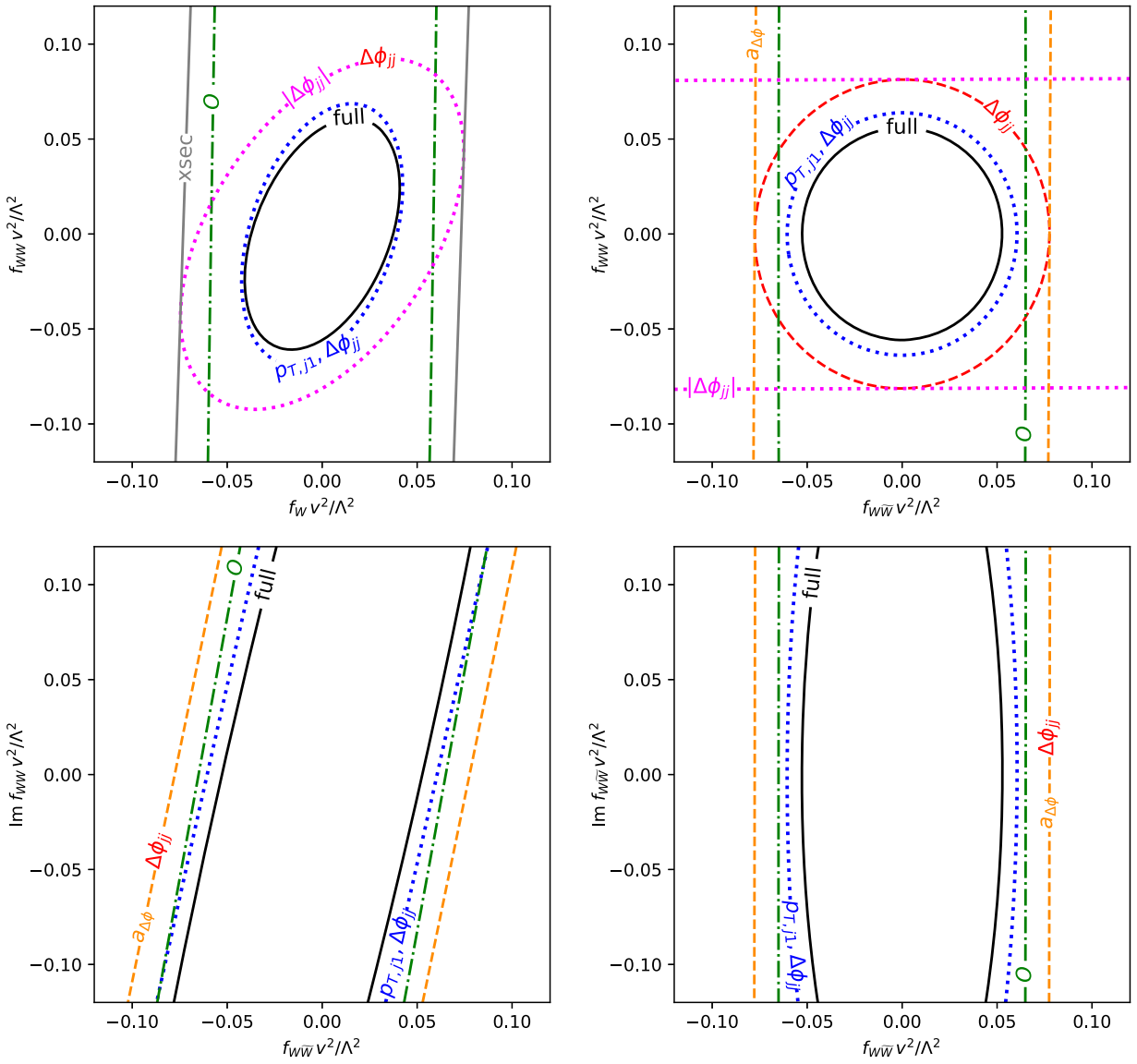

FIG. 3. Optimal 1σ contours for WBF Higgs production with $H \to \tau\tau$ (solid black). Also shown are the results based on different subsets of the $\Delta\phi_{jj}$ distribution, including its absolute value (purple), its asymmetry (orange), its full distribution (red), its combination with the leading jet p_T distribution (blue); as well as the observable O as defined in Eq. (23) (green). In grey we show bounds based on a simple rate measurement. In each panel, the parameters not shown are set to zero.

The case of absorptive physics, represented by a complex phase in the Wilson coefficient, is shown in the lower two panels of Fig. 3. While there is some sensitivity to the imaginary parts of f_{WW} and $f_{W\tilde{W}}$, the reach is typically much weaker for their imaginary parts than for the real parts. Crucially, the lower left panel of Fig. 3 demonstrates that once we allow for such an absorptive phase, an almost blind direction in parameter space arises: none of the observables can unequivocally prove *CP* violation. However, the numerical effect of this correlation on the measurement of the proper Wilson coefficient $f_{W\tilde{W}}$ is not large.

To summarize, *CP*-violating scenarios can lead to large asymmetries in the signed $\Delta\phi_{jj}$ distribution in WBF, giving an impressive new physics reach of the LHC in these signatures. But this genuine $\hat{T}$-odd observable can only be interpreted as a sign of *CP* violation under the additional assumption that rescattering is negligible. While this statement is crucial to understand the model-independence of our *CP*-measurement, the numerical impact of absorptive imaginary parts on the extraction of proper Wilson coefficients it not large. As a side remark, an essentially equivalent measurement is possible for Higgs plus two jets production in gluon fusion, testing the *CP* nature of the effective Higgs interaction with gluons [15].

III. *ZH* PRODUCTION

At the amplitude level and assuming custodial symmetry, the *ZH* signature is sensitive to the same EFT vertices as

WBF production [10]. However, its $q\bar{q}$ initial state is CP-even in the center-of-mass frame and at leading order in QCD. Following Sec. I B this implies that one can construct a genuine CP-odd observable [11]. It thus eschews the need for additional theory assumptions concerning absorptive phases in the Wilson coefficients.

We focus on the case with a leptonic Z decay and Higgs decaying into bottom quarks,

$$q\bar{q} \to ZH \to \ell^-\ell^+ b\bar{b}, \tag{32}$$

which allows us to reconstruct the final state with great precision including the electric charges of the two leptons, which opens the door to C-sensitive observables. The specific Higgs decay $H \to b\bar{b}$ has a large branching ratio, but will not play an important role in our analysis aside from providing information about the initial state momenta.

A. *CP* observables

Once again, the lack of access to spins of any of the participants implies that all realistic observables are constructed from 4-momenta. Following Sec. I C, they have the same transformation properties under P and $\hat{T}$, so a CP-odd observable is either $\hat{T}$-odd, P-odd, and C-even, or it is $\hat{T}$-even, P-even and C-odd. There are two types of CP observables distinguished by their transformation under $\hat{T}$:

(1) CP-odd and $\hat{T}$-odd: as discussed in Sec. I B, there is one P-odd, C-even observable based on the four independent 4-momenta,

$$O_1 = \epsilon_{\mu\nu\rho\sigma} k_1^\mu k_2^\nu q_{\ell^+}^\rho q_{\ell^-}^\sigma \text{sign}((k_1 - k_2)\cdot(q_1 - q_2)), \tag{33}$$

where $k_{1,2}$ are the initial parton momenta and q_{ℓ^+,ℓ^-} are the outgoing ℓ^+ and ℓ^- momenta. As before, the sign ensures that the observable is independent of the parton momenta assignment and C-even. As in Eqs. (21) and (23), O_1 can be related to the azimuthal angle, for which a sign imposes an ordering according to the lepton momentum in the center-of-mass frame.

$$O_1 \to \Delta\phi_{\ell\ell} \equiv (\phi_{\ell^+} - \phi_{\ell^-})\text{sign}(q_{z,\ell^+} - q_{z,\ell^-})_{\text{cm}}. \tag{34}$$

(2) CP-odd and $\hat{T}$-even: the two C-odd observables are constructed from scalar products between a C-even and a C-odd 4-vector. The C-eigenstate 4-vectors are differences of the 4-momenta,

$$k_\pm \equiv k_1 \pm k_2 \xrightarrow{C} \pm k_\pm, \qquad q_\pm \equiv q_{\ell^+} \pm q_{\ell^-} \xrightarrow{C} \pm q_\pm. \tag{35}$$

Because $(k_+ \cdot k_-) = (q_+ \cdot q_-) = 0$ for massless fermions, there are two C-odd scalar products $(q_- \cdot k_+)$ and $(k_- \cdot q_+)$, and the remaining four scalar products are C-even. The first C-odd scalar product maps on to the energy difference between the leptons,

$$O_2 \equiv q_- \cdot k_+ = \sqrt{s}(E_{\ell^+} - E_{\ell^-}) \to (E_{\ell^+} - E_{\ell^-}) \equiv \Delta E_{\ell\ell}, \tag{36}$$

where in the center-of-mass frame $k_{1,2} = (E, 0, 0, \pm E)$, $q_{\ell^\pm} = (E_{\ell^\pm}, \vec{q}_{T,\ell^\pm}, q_{z,\ell^\pm})$, and $s = 4E^2$. The observable $(k_- \cdot q_+)$ is a challenge at the LHC, because there is no practical way to identify the initial state quarks and antiquarks on an event-by-event basis. However, the C-odd combination,

$$\begin{aligned} O_3 &\equiv (q_- \cdot k_+)(q_+ \cdot k_+) - (q_+ \cdot k_-)(q_- \cdot k_-) \\ &= s(q_{T,\ell^+} - q_{T,\ell^-})(q_{T,\ell^+} + q_{T,\ell^-}) \\ &\to (q_{T,\ell^+} - q_{T,\ell^-}) \equiv \Delta p_{T,\ell\ell}, \end{aligned} \tag{37}$$

accesses its information, while only depending on the transverse momentum difference of the leptons [11] and the center of mass energy, which can be determined once the Higgs momentum is reconstructed from its decay products.

Following the discussion in Sec. I A, only the $\hat{T}$-odd observables O_1 or equivalently $\Delta\phi_{\ell\ell}$ probe the CP nature of the Higgs-gauge sector. We illustrate this in the left panel of Fig. 4, which shows the distribution of $\Delta\phi_{\ell\ell}$ for the ZH signal in the SM and with different choices of Wilson coefficients in the EFT. As expected, the CP-odd operator $\mathcal{O}_{W\tilde{W}}$ induces an asymmetry under $\Delta\phi_{\ell\ell} \to -\Delta\phi_{\ell\ell}$. Unlike in WBF, this genuine signature of CP violation cannot be generated from an absorptive phase in CP-even physics.

As discussed in Sec. I A, the $\hat{T}$-even observables O_2 and O_3 or equivalently $\Delta E_{\ell\ell}$ and $\Delta p_{T,\ell\ell}$ will have a nonzero expectation value only in the presence of CP violation and rescattering. The right panel of Fig. 4 shows the distribution of $\Delta E_{\ell\ell}$, demonstrating that an asymmetry in this observable requires both, CP violation and a source of a complex phase.

B. LHC reach

The signature consists of two b-tagged jets and two opposite-sign, same-flavor leptons. We simulate it as in Sec. II, with the b-jet momenta smeared appropriately for the reconstruction in the $H \to b\bar{b}$ decay mode with a Gaussian with width $\sigma_{bb} = 12.5$ GeV [43]. The basic acceptance cuts,

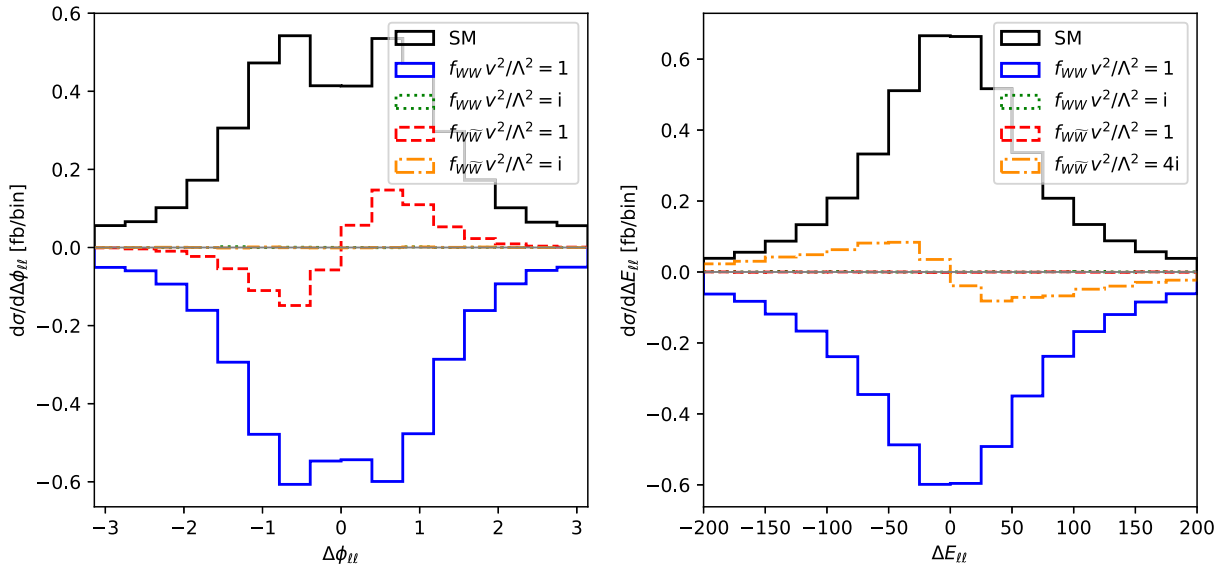

FIG. 4. Distributions of $\Delta\phi_{\ell\ell}$ (left) and $\Delta E_{\ell\ell}$ (right) in ZH production after the cuts in Eqs. (38) and (40) for the Standard Model signal (solid black), and for the interference between different dimension-six amplitudes with the SM signal (colored).

$$\begin{aligned} &p_{T,b} > 20\ \text{GeV} \qquad |\eta_b| < 2.5 \qquad 100\ \text{GeV} < m_{bb} < 150\ \text{GeV} \qquad \Delta R_{bb} > 0.4 \\ &p_{T,\ell} > 10\ \text{GeV} \qquad |\eta_\ell| < 2.5 \qquad 86\ \text{GeV} < m_{\ell\ell} < 96\ \text{GeV} \qquad \Delta R_{\ell\ell}, \Delta R_{\ell b} > 0.4, \end{aligned} \tag{38}$$

include a narrow invariant mass window for the two leptons to effectively reject background processes without an on-shell $Z \to \ell\ell$ decay. After the leptonic invariant mass cut, the main background is the irreducible $b\bar{b}Z_\ell$ production, where the two b-jets are produced as hadronic radiation. The acceptance cuts of Eq. (38) reduce its rate to 629 fb (before b-tagging), to be compared to the SM ZH signal rate of 14 fb.

We require two b-tags. This helps with fake backgrounds (as explained below), but differs with regard to some of the current experimental strategies grappling with limited statistics—a challenge that is much less of a concern with 100 fb^{-1}. We assume a double b-tagging rate for the signal and primary background of 0.7^2. Through mis-tagging, the fake QCD background $gg \to c\bar{c}Z_\ell$ will also contribute. Its rate after the acceptance cuts is 423 fb, and as long as the rate to mis-tag a charm as a b remains below 20%, it is small enough to be ignored. There is also a contribution from mistagged light-flavor jets. Starting from a jjZ_ℓ rate of 17.2 pb after acceptance cuts and applying a mistag probability below 1% it turns out to be negligible.

Pairs of top quarks lead to a final state $b\bar{b}\ell\ell\nu\bar{\nu}$ which is primarily distinguished from the signal by the presence of significant $\not{E}_T$. Supplementing the acceptance cuts with [11,50]

$$\not{E}_T < 20\ \text{GeV} \tag{39}$$

results in a rate of 13 fb before b-tagging. A multivariate analysis of the multiparticle final state will further suppress it to a level where it does not affect the measurement.

After the acceptance cuts, requiring two b-tags, and the $\not{E}_T$ cut, the only relevant background is therefore $b\bar{b}Z_\ell$ production. As in the WBF analysis, we improve the signal extraction through the likelihood-based event selection [29],

$$\frac{\Delta\sigma_{\text{SM}\,ZH}(\mathbf{x})}{\Delta\sigma_{\text{backgrounds}}(\mathbf{x})} > 0.1. \tag{40}$$

The lower cutoff choice relative to WBF is dictated by the larger background rates for the ZH case in the relevant phase-space regions.

With $L = 100$ fb^{-1} of data and after the event selection of Eqs. (38), (39), (40), and all efficiencies, we expect a ZH signal of 208 events in the Standard Model and a total expected background of 1035 events. Our idealized treatment of the detector response and omission of subleading backgrounds mean that these numbers are certainly optimistic.

In the basis of Eq. (12), the Fisher information matrix evaluated at the Standard Model with an integrated luminosity of $L = 100$ fb^{-1} is

$$I_{ij} = \begin{array}{c} \begin{matrix} f_{\phi,2} & f_W & f_B & f_{WW} & f_{BB} & f_{W\widetilde{W}} & f_{B\tilde{B}} & \mathrm{Im}\, f_W & \mathrm{Im}\, f_B & \mathrm{Im}\, f_{WW} & \mathrm{Im}\, f_{BB} & \mathrm{Im}\, f_{W\widetilde{W}} & \mathrm{Im}\, f_{B\tilde{B}} \end{matrix} \\ \begin{pmatrix} 4971.9 & 844.2 & 257.5 & 447.0 & 41.6 & 0.4 & 0.0 & 0.3 & 0.1 & -0.4 & 0.0 & -0.1 & 0.0 \\ 844.2 & 858.5 & 261.8 & 174.2 & 16.2 & 0.3 & 0.0 & -0.1 & 0.0 & 0.2 & 0.0 & 0.3 & 0.0 \\ 257.5 & 261.8 & 79.8 & 53.1 & 4.9 & 0.1 & 0.0 & 0.0 & 0.0 & 0.1 & 0.0 & 0.1 & 0.0 \\ 447.0 & 174.2 & 53.1 & 65.8 & 6.1 & 0.1 & 0.0 & 0.0 & 0.0 & 0.0 & 0.0 & 0.0 & 0.0 \\ 41.6 & 16.2 & 4.9 & 6.1 & 0.6 & 0.0 & 0.0 & 0.0 & 0.0 & 0.0 & 0.0 & 0.0 & 0.0 \\ 0.4 & 0.3 & 0.1 & 0.1 & 0.0 & 5.3 & 0.5 & 0.0 & 0.0 & 0.0 & 0.0 & 0.0 & 0.0 \\ 0.0 & 0.0 & 0.0 & 0.0 & 0.0 & 0.5 & 0.0 & 0.0 & 0.0 & 0.0 & 0.0 & 0.0 & 0.0 \\ 0.3 & -0.1 & 0.0 & 0.0 & 0.0 & 0.0 & 0.0 & 5.1 & 1.6 & -7.8 & -0.7 & 0.0 & 0.0 \\ 0.1 & 0.0 & 0.0 & 0.0 & 0.0 & 0.0 & 0.0 & 1.6 & 0.5 & -2.4 & -0.2 & 0.0 & 0.0 \\ -0.4 & 0.2 & 0.1 & 0.0 & 0.0 & 0.0 & 0.0 & -7.8 & -2.4 & 12.0 & 1.1 & 0.0 & 0.0 \\ 0.0 & 0.0 & 0.0 & 0.0 & 0.0 & 0.0 & 0.0 & -0.7 & -0.2 & 1.1 & 0.1 & 0.0 & 0.0 \\ -0.1 & 0.3 & 0.1 & 0.0 & 0.0 & 0.0 & 0.0 & 0.0 & 0.0 & 0.0 & 0.0 & 16.2 & 1.5 \\ 0.0 & 0.0 & 0.0 & 0.0 & 0.0 & 0.0 & 0.0 & 0.0 & 0.0 & 0.0 & 0.0 & 1.5 & 0.1 \end{pmatrix} \end{array} \begin{matrix} f_{\phi,2} \\ f_W \\ f_B \\ f_{WW} \\ f_{BB} \\ f_{W\widetilde{W}} \\ f_{B\tilde{B}} \\ \mathrm{Im}\, f_W \\ \mathrm{Im}\, f_B \\ \mathrm{Im}\, f_{WW} \\ \mathrm{Im}\, f_{BB} \\ \mathrm{Im}\, f_{W\widetilde{W}} \\ \mathrm{Im}\, f_{B\tilde{B}} \end{matrix}, \quad (41)$$

with CP-odd components highlighted in red. Again we stress that the results for the real Wilson coefficients is independent of the toy model assumptions underlying the imaginary components.

This is translated into optimal error contours in Fig. 5, where each panel shows a pair of Wilson coefficients, with the remaining ones set to zero. In addition to the bounds based on the full kinematic information, we also show the optimal constraints based on individual observables. Once again, the best constraints on the CP-even operators come from a combination of angular observables like $\Delta\phi_{\ell\ell}$ and momentum-sensitive observables like m_{ZH}. The ZH production processes turns out to offer much tighter constraints on f_W than f_{WW}.

The distribution of $\Delta\phi_{\ell\ell}$ is sensitive to both CP-even and CP-violating operators. Unsurprisingly, the information on CP-even operators is entirely contained in the absolute value $|\Delta\phi_{\ell\ell}|$. In contrast, the differential asymmetry

$$a_{\Delta\phi_{\ell\ell}} \equiv \frac{\mathrm{d}\sigma(\Delta\phi_{\ell\ell}) - \mathrm{d}\sigma(-\Delta\phi_{\ell\ell})}{\mathrm{d}\sigma(\Delta\phi_{\ell\ell}) + \mathrm{d}\sigma(-\Delta\phi_{\ell\ell})}, \quad (42)$$

carries all of the information concerning CP violation. Unlike $\Delta\phi_{jj}$ in WBF, it is now a genuine CP-odd observable, so this asymmetry is never generated from real or imaginary Wilson coefficients of CP-even operators, and the lower left panel of Fig. 5 does not suffer from blind directions.

As expected from the discussion in Sec. I B, the distributions of $\Delta p_{T,\ell\ell}$ and $\Delta E_{\ell\ell}$ can only exhibit asymmetries if both CP violation and absorptive phases are present. This leads to these distributions only being sensitive to the imaginary part of $\mathcal{O}_{W\tilde{W}}$, as is visible in the bottom right panel of Fig. 5.

Altogether, we find that ZH production with its CP-even initial state provides us with genuine CP-odd observables that do not rely on any further theory assumptions. In particular the signed azimuthal angle difference $\Delta\phi_{\ell\ell}$ provides a clean probe of the CP nature of the Higgs-gauge sector. Unfortunately, the small rate and large backgrounds limit the new physics reach of the LHC in this channel.

IV. $H \to 4$ LEPTONS

The final, classic [13,14] process we consider is the Higgs decaying into four leptons, which offers full reconstruction of the final state, including all of the electric charges. On the other hand, in this process the Higgs is almost always on-shell, limiting the momentum flow through the HZZ vertex. In addition, the fact that one of the Z bosons is typically on-shell results in one less independent degree of freedom in the favored region of kinematics. Nevertheless, the four leptons in the final state can be reconstructed with exquisite precision, which might help compensate for the smaller lever arm in energy.

The four leptons are organized into two same-flavor, opposite-sign pairs, whose momenta are labeled as:

$$H \to \ell_1^+(q_{11})\ell_1^-(q_{12})\ell_2^+(q_{21})\ell_2^-(q_{22}). \quad (43)$$

where $\ell_{1,2} = e, \mu$ are restricted to electrons and muons which can be reconstructed very precisely. Even combined with the relatively featureless gluon-fusion Higgs production mode, this decay mode has essentially no backgrounds and is largely statistics limited.

A. CP observables

Once again, the lack of spin information dictates that all observables are constructed from the 4-momenta, and transformation the same way under both P and $\hat{T}$. Thus, as for ZH production, any CP-odd observable is either $\hat{T}$-odd, C-even, and P-odd and or $\hat{T}$-even, C-odd, and

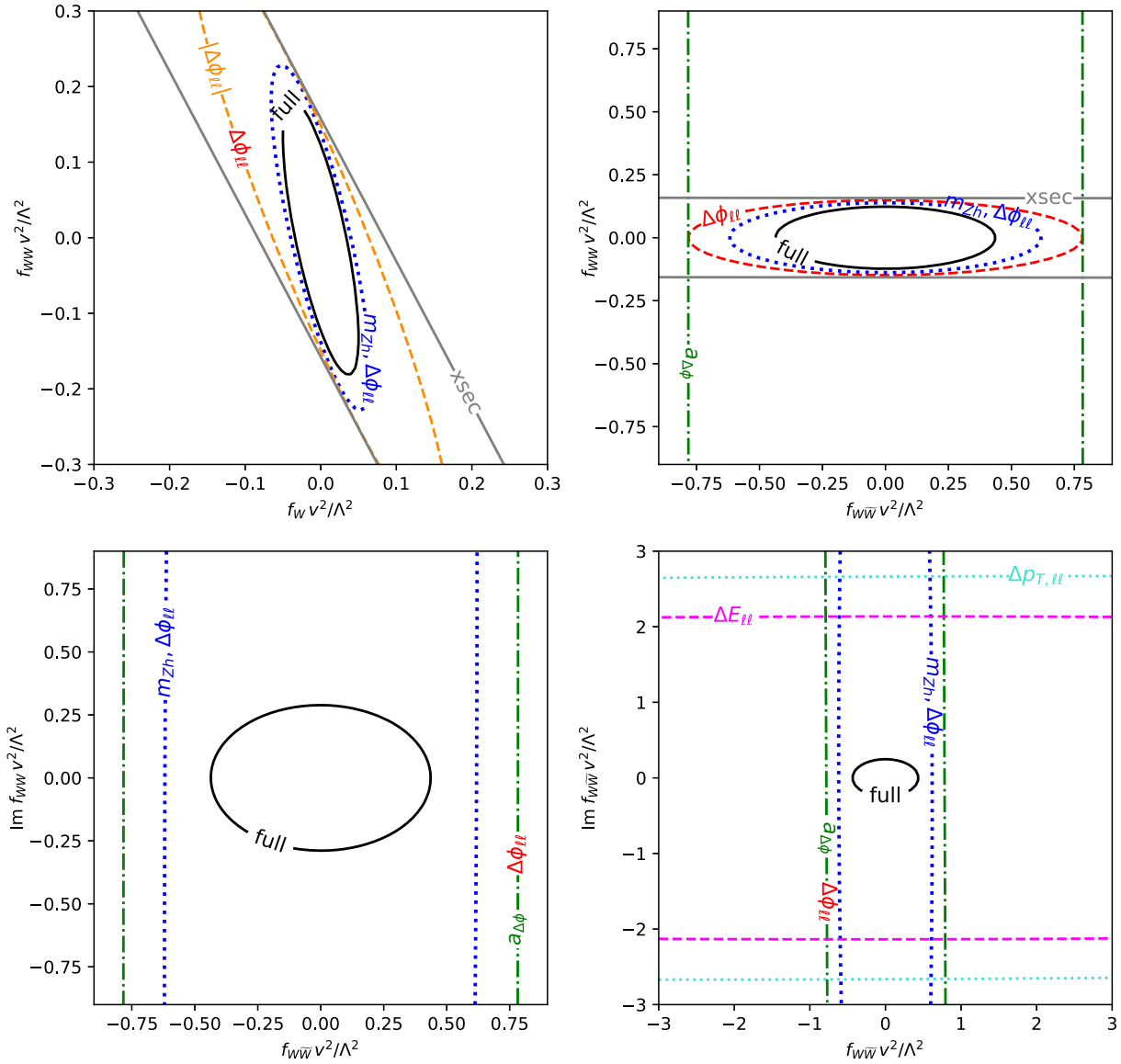

FIG. 5. Optimal 1σ contours for ZH production (solid black). The colored lines show the reach contained in the $\Delta\phi_{\ell\ell}$ distribution, including its absolute value (orange), asymmetry (green), full distribution (red), combination with the m_{ZH} distribution (blue); based on the distribution of $\Delta E_{\ell\ell}$ (purple); for the distribution of $\Delta p_{T,\ell\ell}$ (turquoise); and based on a simple rate measurement (grey). In each panel, the parameters not shown are set to zero.

P-even. The initial state, at leading order, is CP-symmetric and $\hat{T}$-symmetric in the Higgs rest or center-of-mass frames. We combine the lepton 4-momenta into C-eigenstates

$$q_{1\pm} = q_{11} \pm q_{12} \qquad q_{2\pm} = q_{21} \pm q_{22}. \tag{44}$$

Similarly to the discussion in Secs. I B and II A, there are two classes of observables:

(1) CP-odd and $\hat{T}$-odd: there is exactly one observable in $H \to 4\ell$ decays that is P-odd and C-even,

$$O_a \equiv 4\epsilon_{\mu\nu\rho\sigma} q_{11}^{\mu} q_{12}^{\nu} q_{21}^{\rho} q_{22}^{\sigma} = \epsilon_{\mu\nu\rho\sigma} q_{1+}^{\mu} q_{1-}^{\nu} q_{2+}^{\rho} q_{2-}^{\sigma}. \tag{45}$$

Unlike in Eq. (20), there is no need for an explicit sign factor to compensate for unobservable permutations. It is convenient to work in the Higgs rest frame with both Z-boson 3-momenta along the z-axis, implying $q_{i+} = (E_i, 0, 0, q_{z,i})$ with $E_1 + E_2 = m_H$ and $q_{z,1} + q_{z,2} = 0$. In this frame,

$$O_a \to m_H (\vec{q}_{1-} \times \vec{q}_{2-}) \cdot \vec{q}_{1+}. \tag{46}$$

We can relate this to the Z-decay plane correlation angle Φ in Eq. (2) of Ref. [19] by introducing $\vec{n}_i = \vec{q}_{i1} \times \vec{q}_{i2}$ and making use of the identity $(\vec{a} \times \vec{b}) \times (\vec{a} \times \vec{c}) = [\vec{a} \cdot (\vec{b} \times \vec{c})]\vec{a}$, leading to

$$O_a = -\frac{16 m_H}{\vec{q}^{\,2}_{1+}} \vec{q}_{1+} \cdot (\vec{n}_1 \times \vec{n}_2) \sim \sin\Phi. \quad (47)$$

Note that in Ref. [19] the definition of the angle between the two Z-decay planes is slightly more complicated. They relate the absolute value of Φ from $\cos\Phi = (\vec{n}_1\vec{n}_2)/|\vec{n}_1\vec{n}_2|$ and extract the sign of the angle from $\mathrm{sign}(\Phi) = \vec{q}_{1+}\cdot(\vec{n}_1\times\vec{n}_2)/(|\vec{q}_{1+}\cdot(\vec{n}_1\times\vec{n}_2)|)$. Since only the latter is sensitive to P violation, its information is equivalent to O_a.

(2) CP-odd and $\hat{T}$-even: as before, we construct two scalar-product-based CP-odd observables by combining C-even and C-odd 4-vectors: $(q_{2+} \cdot q_{1-})$ and $(q_{1+} \cdot q_{2-})$. In the rest frame of q_{1+} we define

$$O_b \equiv -(q_{2+} \cdot q_{1-}) = 2|\vec{q}_{2+}||\vec{q}_{11}|\cos\theta_1, \quad (48)$$

with the same angle θ_1 as in Ref. [19]. Similarly, in the q_{2+} rest frame, we define

$$O_c \equiv -(q_{1+} \cdot q_{2-}) = 2|\vec{q}_{1+}||\vec{q}_{21}|\cos\theta_2. \quad (49)$$

The relation between these decay angles and the tagging jet correlation in WBF is well known [22,35]. Because the effects of dimension-six operators are enhanced at higher momentum transfer, selections on the invariant masses q^2_{1+} and q^2_{2+} can enhance the sensitivity to CP-violating operators, even though these variables themselves are not sensitive to CP violation.

B. LHC reach

We simulate the signature,

$$pp \to H \to \ell_1^+\ell_1^-\ell_2^+\ell_2^-, \quad (50)$$

with two pairs of opposite-sign, same-flavor leptons $\ell_{1,2} = e, \mu$. We apply the basic event selection

$$p_{T,\ell} > 10\ \mathrm{GeV} \qquad |\eta_\ell| < 2.5$$
$$120\ \mathrm{GeV} < m_{4\ell} < 130\ \mathrm{GeV}. \quad (51)$$

After these cuts, there is a small background from continuum ZZ production, which we include with an appropriate smearing of the $m_{4\ell}$ invariant masses.

As before, we assume an integrated luminosity of 100 fb^{-1} and neglect the detector efficiencies for the four leptons. For the Wilson coefficients given in Eq. (12), we find the following Fisher information matrix evaluated at the Standard Model, with CP-odd components in red:

$$I_{ij} = \begin{array}{c} \begin{array}{cccccccccccccc} f_{\phi,2} & f_W & f_B & f_{WW} & f_{BB} & f_{W\widetilde{W}} & f_{B\tilde{B}} & \mathrm{Im}\, f_W & \mathrm{Im}\, f_B & \mathrm{Im}\, f_{WW} & \mathrm{Im}\, f_{BB} & \mathrm{Im}\, f_{W\widetilde{W}} & \mathrm{Im}\, f_{B\tilde{B}} & \end{array} \\ \begin{pmatrix} 1649.4 & 135.1 & 41.4 & -69.7 & -6.4 & 0.3 & 0.1 & -1.4 & 0.3 & 2.1 & -0.1 & -0.2 & 0.1 \\ 135.1 & 11.4 & 3.5 & -6.2 & -0.5 & 0.0 & 0.0 & -0.1 & 0.0 & 0.2 & 0.0 & 0.0 & 0.0 \\ 41.4 & 3.5 & 1.1 & -1.8 & -0.2 & 0.0 & 0.0 & 0.0 & 0.0 & 0.0 & 0.0 & 0.0 & 0.0 \\ -69.7 & -6.2 & -1.8 & 3.9 & 0.3 & 0.0 & 0.0 & 0.1 & 0.0 & -0.1 & 0.0 & 0.0 & 0.0 \\ -6.4 & -0.5 & -0.2 & 0.3 & 0.2 & 0.0 & 0.0 & 0.0 & 0.0 & 0.0 & 0.0 & 0.0 & 0.0 \\ 0.3 & 0.0 & 0.0 & 0.0 & 0.0 & 0.5 & -0.1 & 0.0 & 0.0 & 0.0 & 0.0 & 0.0 & 0.0 \\ 0.1 & 0.0 & 0.0 & 0.0 & 0.0 & -0.1 & 0.1 & 0.0 & 0.0 & 0.0 & 0.0 & 0.0 & 0.0 \\ -1.4 & -0.1 & 0.0 & 0.1 & 0.0 & 0.0 & 0.0 & 0.0 & 0.0 & -0.1 & 0.0 & 0.0 & 0.0 \\ 0.3 & 0.0 & 0.0 & 0.0 & 0.0 & 0.0 & 0.0 & 0.0 & 0.0 & 0.1 & 0.0 & 0.0 & 0.0 \\ 2.1 & 0.2 & 0.0 & -0.1 & 0.0 & 0.0 & 0.0 & -0.1 & 0.1 & 0.3 & 0.0 & 0.0 & 0.0 \\ -0.1 & 0.0 & 0.0 & 0.0 & 0.0 & 0.0 & 0.0 & 0.0 & 0.0 & 0.0 & 0.1 & 0.0 & 0.0 \\ -0.2 & 0.0 & 0.0 & 0.0 & 0.0 & 0.0 & 0.0 & 0.0 & 0.0 & 0.0 & 0.0 & 0.4 & 0.0 \\ 0.1 & 0.0 & 0.0 & 0.0 & 0.0 & 0.0 & 0.0 & 0.0 & 0.0 & 0.0 & 0.0 & 0.0 & 0.1 \end{pmatrix} \begin{array}{c} f_{\phi,2} \\ f_W \\ f_B \\ f_{WW} \\ f_{BB} \\ f_{W\widetilde{W}} \\ f_{B\tilde{B}} \\ \mathrm{Im}\, f_W \\ \mathrm{Im}\, f_B \\ \mathrm{Im}\, f_{WW} \\ \mathrm{Im}\, f_{BB} \\ \mathrm{Im}\, f_{W\widetilde{W}} \\ \mathrm{Im}\, f_{B\tilde{B}} \end{array} \end{array} . \quad (52)$$

The results for the real Wilson coefficients are again unaffected by the toy model assumptions that underly the imaginary parts.

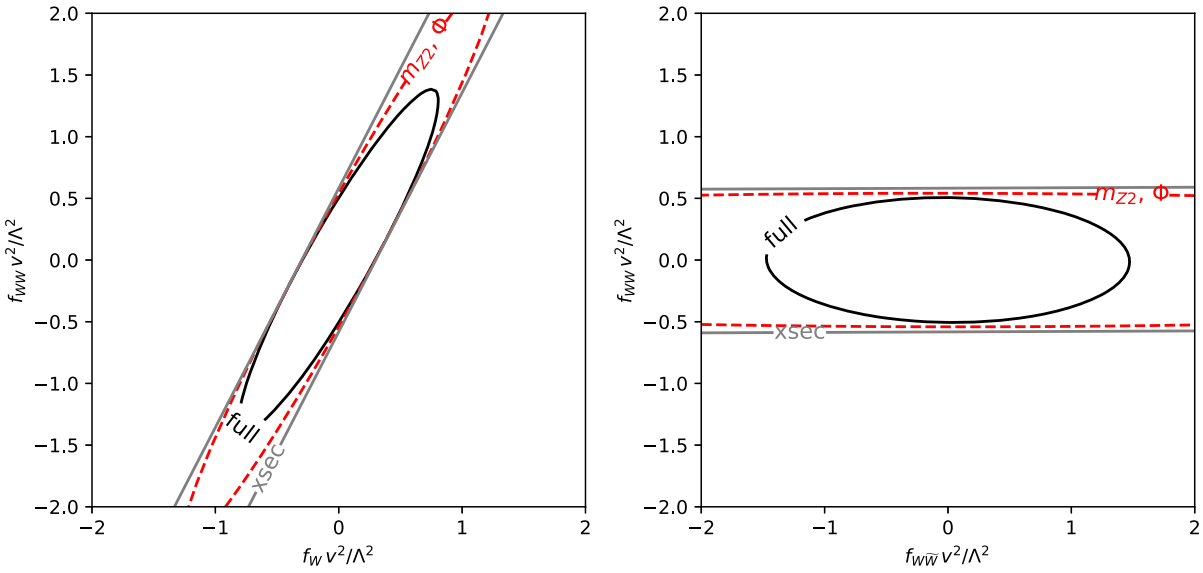

FIG. 6. Optimal 1σ contours for $gg \to h \to 4\ell$ (solid black). In grey we show bounds based on a rate measurement. The red line shows the contours based on an analysis of the lower of the two lepton pair masses m_{Z_2} and Φ, other kinematic variables lead to bounds between the red and grey lines. In each panel, the parameters not shown are set to zero.

Optimal exclusion limits for representative pairs of Wilson coefficients are shown in Fig. 6. The sensitivity is about 10 times worse for $H \to 4\ell$ than for ZH or WBF production, indicating that the enhanced precision in measuring the lepton momenta does not overcome the limitations of the restricted momentum transfer and dominantly constrained kinematics.

V. COMPARISON AND SUMMARY

The presence of new sources of *CP* violation in the Higgs sector is of fundamental importance and, according to some common lore, may shed light on mysteries such as the baryon asymmetry of the Universe. It is crucial to establish the symmetry structure through well-defined observables as an ingredient to a global analysis, for example a dimension-six effective field theory containing both *CP*-conserving and *CP*-violating operators.

We have examined *CP*-sensitive observables in WBF Higgs production, ZH production, and Higgs decays into four leptons. While the underlying hard processes, and hence the sensitivity to the *CP* properties of the Higgs-gauge sector, are essentially identical for the three processes, the different initial and final state assignments define distinct signatures:

(1) For WBF, the initial state is not a *CP* eigenstate and one cannot measure the charges of initial-state or final-state quarks. In this situation, we can use the naive time reversal to test the underlying *CP* properties, but only under the assumption of no rescattering effects. On the other hand, the momentum flow through the Higgs vertex can be large.

(2) In ZH production, the initial state is a *CP* eigenstate at leading order and one can easily identify the lepton charges in the final state. We can construct a genuine *CP*-odd observable, which directly reflects the *CP* symmetry of the underlying Lagrangian without any assumptions and without any additional complex phases. The momentum flow through the Higgs vertex can be enhanced by kinematic cuts.

(3) Finally, for $H \to e^+e^-\mu^+\mu^-$, one has full control over the kinematics of the process, allowing for a straightforward construction of *CP*-sensitive observables. However, the momentum flow through the relevant Higgs vertex is restricted by the Higgs mass and one of the Z-bosons is on-shell, limiting the kinematic coverage of the process.

In a next step, we have analyzed the new physics reach of the processes and observables in terms of thirteen Wilson coefficients. By calculating the Fisher information in the different signatures, we determined the optimal possible exclusion limits at the LHC, including through any multivariate analysis and taking into account all correlations between different operators.

The results of this comprehensive comparison are summarized in Fig. 7. We compare the optimal sensitivity of the three analyzed channels when either performing a fully multivariate analysis or a histogram-based analysis of either one or a combination of two kinematic distributions, assuming an integrated luminosity of 100 fb^{-1}. In the top panel, we show the eigenvalues and eigenvectors of the Fisher information matrices. The colors denote the decomposition of the corresponding eigenvectors, defining the direction of a given eigenvector in model parameter space.

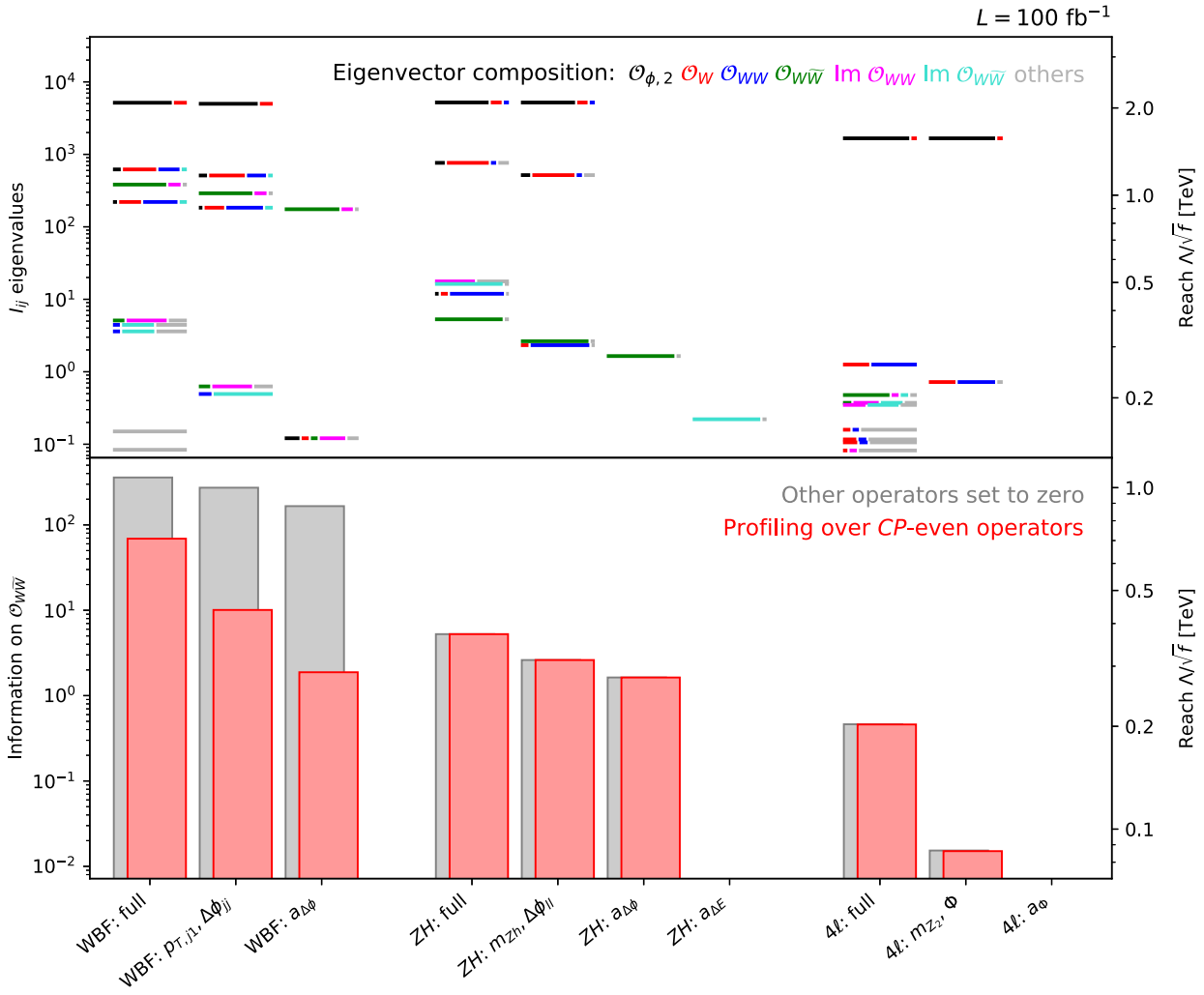

FIG. 7. Comparison of the sensitivity of different channels and observables at the LHC with 100 fb^{-1}. In the top panel we show the eigenvalues of the various Fisher information matrices. The colors denote the decomposition of the corresponding eigenvectors: the length of each segment is proportional to the magnitude of the eigenvector component. In the bottom panel we show the Fisher information on the CP-violating Wilson coefficient $f_{W\tilde{W}}$. The grey bars show the sensitivity assuming that all other considered operators are zero, while the red bars profile over arbitrary values of all of the CP-even parameters (including absorptive parts). In both panels, the right axes translate the Fisher information into the corresponding new physics reach.

The right axis translates the corresponding Fisher information into the new physics reach along this direction in model parameter space.

In general, the CP-even operator $\mathcal{O}_{\phi,2}$, which rescales all Higgs couplings, dominates the most sensitive directions for all three processes [29], typically followed by a combination of $\mathcal{O}_W$ and $\mathcal{O}_{WW}$. Of the two CP-odd operators $\mathcal{O}_{W\tilde{W}}$ and $\mathcal{O}_{B\tilde{B}}$, only the former can be meaningfully constrained in these processes. In WBF Higgs production, the sensitivity to this operator is best isolated in the asymmetry $a_{\Delta\phi}$, which is not sensitive to any real CP-even Wilson coefficients. But the corresponding Fisher information still shows an admixture mixture of the imaginary Wilson coefficient of the CP-even operator $\mathcal{O}_{WW}$, once again demonstrating that additional theory assumptions are necessary to measure CP violation in this channel. In contrast, the genuine CP-odd asymmetry $a_{\Delta\phi}$ in ZH production is solely sensitive to CP-violating operators, albeit at a reduced new physics reach. As expected, the asymmetry $a_{\Delta E}$ is sensitive only to the combination of CP violation and absorptive physics modelled by imaginary coefficients for the operator $\mathcal{O}_{W\tilde{W}}$. Note that such absorptive parts are not generated by integrating out heavy particles and are therefore not present in an effective theory, but we use them as a toy model to illustrate the potential effect of light new states.

In both WBF and ZH production, adding observables that measure the momentum transfer significantly increases the information on all operators, but at the cost of obfuscating the CP interpretation of the results. Finally, the Higgs decay is only really sensitive to the combination of mostly $\mathcal{O}_{\phi,2}$ and $\mathcal{O}_W$ that affects the total rate in this

channel, and the physics reach in any other direction in model space is severely hampered by the limited momentum flow.

In the bottom panel, we focus on the Fisher information on the *CP*-violating Wilson coefficient $f_{W\tilde{W}}$. The grey bars show the sensitivity assuming that all other considered operators are zero, translated into the new physics reach on the right axis. A combination of the two leading WBF observables p_{T,j_1} and $\Delta\phi_{jj}$ [15] captures almost the entire phase-space information on $f_{W\tilde{W}}$ when other operators are not taken into account. When we profile over arbitrary values of all of the *CP*-even parameters, this feature gets washed out, motivating a multivariate WBF analysis. The theoretically better-controlled *ZH* production channel has a significantly smaller reach than the WBF signature, but its reach for $f_{W\tilde{W}}$ is literally unaffected by other operators, thanks to the genuine *CP*-odd observable. For the Higgs decay, the only news which is worse than the fact that there is very little information distributed over phase space is that the genuine *CP*-odd asymmetry a_Φ is extremely limited in reach.

Altogether, we find that a *CP* measurement in WBF production provides the best reach, but its interpretation is theoretically not very clean. A *CP* measurement in *ZH* production is less model-dependent and more stable in terms of correlations, because we can construct an appropriate genuine *CP*-odd observable. In both cases, variables constructed to be sensitive to *CP* can be combined with information pertaining to the momentum transfer, which enhances the effect of dimension-six operators compared to the Standard Model amplitude. Finally, the Higgs decay is easily reconstructed and analyzed, but has a very limited reach because of its limited momentum transfer. Between the three processes we studied, there is no unequivocally best signature to determine the *CP* properties of the Higgs-gauge sector, but there is clearly a worst.

ACKNOWLEDGMENTS

We would like to thank Kyle Cranmer, whose ideas laid the foundation for our information-based approach to particle physics. We would like to thank Fabio Maltoni for his useful comments on the manuscript. T. M. P. T. has benefited from conversations with Christoph Weniger. J. B. is grateful for the support of the Moore-Sloan Data Science Environment at New York University. The work of F. K. and T. M. P. T. is supported in part by National Science Foundation under Grant No. PHY-1620638. T. P. is supported by the DFG Forschergruppe *New Physics at the LHC* (FOR 2239). The authors acknowledge support by the state of Baden-Württemberg through bwHPC.

APPENDIX: ANALYTIC FORM OF THE CROSS SECTION

The most general Lorentz structure of the Higgs-gauge couplings $HV^\alpha(k_1)V^\beta(k_2)$ for on-shell gauge bosons can be written as [19,22,51]

$$T^{\alpha\beta} = \frac{2i}{v}[a_V m_V^2 g^{\alpha\beta} + b_V(k_2^\alpha k_1^\beta - k_1\cdot k_2 g^{\alpha\beta}) + \beta_V \epsilon^{\alpha\beta\gamma\delta} k_{1\gamma} k_{2\delta}]. \tag{A1}$$

The SM at tree level is characterized by $a = 1$ and $b = \beta = 0$. Radiative corrections in the SM or new light new particles can introduce complex phases in a, b and β. In the Standard Model EFT, we can relate a, b and β to the Wilson coefficients of the dimension-six operators,

$$a_W = 1 + m_W^2 \frac{f_W}{\Lambda^2} \qquad b_W = -m_W^2\left(\frac{f_W}{\Lambda^2} + 2\frac{f_{WW}}{\Lambda^2}\right)$$
$$\beta_W = m_W^2 \frac{f_{W\tilde{W}}}{\Lambda^2}, \tag{A2}$$

and similar for the *HZZ* couplings. These couplings are constrained by Higgs measurements. In particular, the decay mode $H \to \gamma\gamma$ is sensitive to new physics contributions, since it first appears at one loop in the SM. The dimension-six operators introduced above induce an additional contribution described by the form factor

$$b_\gamma = -m_W^2 s_W^2 \frac{f_{WW} + f_{BB}}{\Lambda^2}. \tag{A3}$$

The absence of deviation from the SM in the di-photon channel therefore implies $f_{BB} \approx -f_{WW}$.

The three processes considered in this paper are at leading order described by the single diagram shown in Fig. 8. We evaluate the corresponding matrix elements for the general form of the Higgs coupling to vector bosons in Eq. (A1), using the *W*-boson mediated WBF Higgs production for illustration. The other processes shown in Fig. 1 are related by appropriate crossings. In this case, the gauge-fermion coupling takes the form $-ig/(2\sqrt{2})\gamma^\mu(1-\gamma^5)V_{qq'}$ where $V_{qq'}$ is the CKM matrix. It is instructive to introduce the combinations

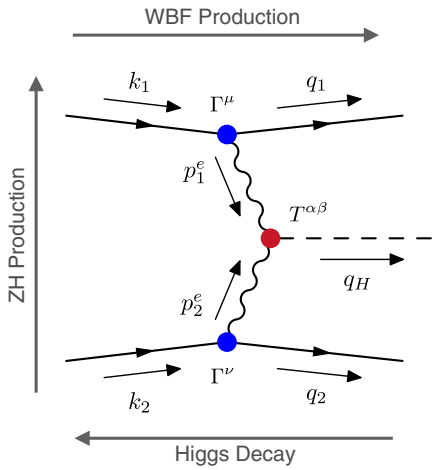

FIG. 8. Feynman diagram for WBF-Higgs production, *ZH* production and Higgs decay to 4 leptons. The arrows indicate the momentum assignment used in the text.

$$p_1^e = p_{11} - p_{12} \qquad p_1^o = p_{11} + p_{12} \qquad p_2^e = p_{21} - p_{22} \qquad p_2^o = p_{21} + p_{22}, \tag{A4}$$

where the p_i^e correspond to the vector boson momenta. In cases of ZH production and $H \to 4\ell$ decay, the momenta p_i^o will be odd under C-conjugation, while the p_i^e are C-even. From these momenta, we construct eleven different Lorentz invariant observables describing the kinematics:

$$\begin{aligned}
C\text{-odd}&: C_1 = p_1^e \cdot p_2^o \qquad C_2 = p_2^e \cdot p_1^o \\
C\text{-even}&: N_1 = p_1^e \cdot p_2^e \qquad N_2 = p_1^e \cdot p_1^e \qquad N_3 = p_1^o \cdot p_2^o \qquad N_4 = p_2^e \cdot p_2^e \\
\text{vanishing}&: V_1 = p_1^e \cdot p_1^o = 0 \qquad V_2 = p_2^e \cdot p_2^o = 0 \\
P\text{-odd}&: P_1 = \epsilon_{\alpha\beta\gamma\delta} p_1^{e\alpha} p_1^{o\beta} p_2^{e\gamma} p_2^{o\delta},
\end{aligned} \tag{A5}$$

where we have used the fact that the fermions are approximately massless. The squared matrix element for the process $ud \to duH$, averaged over initial spins and summed over final spins, takes the form

$$\begin{aligned}
|\mathcal{M}|^2 &= \frac{g^4 |V_{ud}|^4}{1024} \frac{N}{(p_1^2 - m_W^2)^2 (p_2^2 - m_W^2)^2} \\
\text{with} \quad N &= |a|^2 f_a + |b|^2 f_b + |\beta|^2 f_\beta + 2\mathrm{Re}(ab^*) f_{ab}^R + 2\mathrm{Im}(ab^*) f_{ab}^I + 2\mathrm{Re}(a\beta^*) f_{a\beta}^R + 2\mathrm{Im}(a\beta^*) f_{a\beta}^I \\
&\quad + 2\mathrm{Re}(b\beta^*) f_{b\beta}^R + 2\mathrm{Im}(b\beta^*) f_{b\beta}^I.
\end{aligned} \tag{A6}$$

The individual contributions are

$$\begin{aligned}
f_a &= m_V^4 ((N_1 + N_3)^2 - (C_1 + C_2)^2) \\
f_b &= (C_1 C_2 - N_1 N_3)^2 + N_2 N_4 (C_1^2 + C_2^2 + 2 N_1 N_3) + N_2^2 N_4^2 \\
f_\beta &= N_2 N_4 (2 C_1 C_2 + N_1^2 + N_3^2) - (C_1 C_2 - N_1 N_3)^2 - N_2^2 N_4^2 \\
f_{ab}^R &= m_V^2 (N_1 + N_3)(C_1 C_2 - N_1 N_3 - N_2 N_4) \\
f_{ab}^I &= m_V^2 P_1 (C_1 + C_2) \\
f_{a\beta}^R &= -m_V^2 P_1 (N_1 + N_3) \\
f_{a\beta}^I &= m_V^2 (C_1 + C_2)(N_1 N_3 + N_2 N_4 - C_1 C_2) \\
f_{b\beta}^R &= P_1 (N_1 N_3 + N_2 N_4 - C_1 C_2) \\
f_{b\beta}^I &= (C_1 + C_2) N_2 N_4 (N_1 + N_3).
\end{aligned} \tag{A7}$$

For a nonvanishing expectation value of the P-odd observable P_1, the squared matrix element must contain a term linear in P_1. Such terms are generated either in the presence of CP-violating new physics, when either $\mathrm{Re}(a\beta^*) \neq 0$ or $\mathrm{Re}(b\beta^*) \neq 0$, or in the presence of the absorptive phase $\mathrm{Im}(ab) \neq 0$.

In the processes involving a Z boson, the process may also enjoy a well-defined transformation under charge conjugation. In this case, a nonvanishing expectation value for the C-odd observables $C_{1,2}$ requires the squared matrix element to contain a term linear in $C_{1,2}$. Such terms are generated only via rescattering effects when $\mathrm{Im}(ab^*), \mathrm{Im}(a\beta^*), \mathrm{Im}(b\beta^*) \neq 0$. The measurement of C_i sometimes requires the identification of fermion charges and, therefore, is not possible for all processes. Note that f_{ab}^I is both C-odd and P-odd and therefore CP-even. Thus, it does not contribute to a nonvanishing expectation value of both P and C_i if the initial state is CP-symmetric, verifying the observation that absorptive phases can induce an asymmetry in P_1 in WBF Higgs production, but not in ZH production or $H \to 4\ell$ decay.

[1] P. W. Higgs, Phys. Lett. **12**, 132 (1964); Phys. Rev. Lett. **13**, 508 (1964); F. Englert and R. Brout, Phys. Rev. Lett. **13**, 321 (1964).

[2] G. Aad *et al.* (ATLAS Collaboration), Phys. Lett. B **716**, 1 (2012); S. Chatrchyan *et al.* (CMS Collaboration), Phys. Lett. B **716**, 30 (2012).

[3] S. Weinberg, Phys. Lett. B **91**, 51 (1980); S. R. Coleman, J. Wess, and B. Zumino, Phys. Rev. **177**, 2239 (1969); C. G. Callan, Jr., S. R. Coleman, J. Wess, and B. Zumino, Phys. Rev. **177**, 2247 (1969).

[4] C. J. C. Burges and H. J. Schnitzer, Nucl. Phys. **B228**, 464 (1983); C. N. Leung, S. T. Love, and S. Rao, Z. Phys. C **31**, 433 (1986); W. Buchmüller and D. Wyler, Nucl. Phys. **B268**, 621 (1986).

[5] For reviews see e.g. M. S. Bilenky and A. Santamaria, Nucl. Phys. **B420**, 47 (1994); G. Buchalla, A. J. Buras, and M. E. Lautenbacher, Rev. Mod. Phys. **68**, 1125 (1996); C. Englert, A. Freitas, M. M. Mühlleitner, T. Plehn, M. Rauch, M. Spira, and K. Walz, J. Phys. G **41**, 113001 (2014).

[6] I. Brivio and M. Trott, arXiv:1706.08945.

[7] For a comprehensive analysis of Run I and LEP data and including weak boson production, see e.g. A. Butter, O. J. P. Eboli, J. Gonzalez-Fraile, M. C. Gonzalez-Garcia, T. Plehn, and M. Rauch, J. High Energy Phys. 07 (2016) 152; A. Falkowski, M. Gonzalez-Alonso, A. Greljo, D. Marzocca, and M. Son, arXiv:1609.06312.

[8] D. de Florian *et al.* (LHC Higgs Cross Section Working Group Collaboration), arXiv:1610.07922.

[9] For a detailed description of an EFT with extended particle content, see e.g. S. Dawson and C. W. Murphy, Phys. Rev. D **96**, 015041 (2017); M. Bauer, A. Butter, J. Gonzalez-Fraile, T. Plehn, and M. Rauch, Phys. Rev. D **95**, 055011 (2017); S. Dawson and C. W. Murphy, Phys. Rev. D **96**, 015041 (2017).

[10] T. Han and Y. Li, Phys. Lett. B **683**, 278 (2010).

[11] N. D. Christensen, T. Han, and Y. Li, Phys. Lett. B **693**, 28 (2010).

[12] For an excellent introduction, see e.g. G. Valencia, in Boulder 1994, Proceedings, *CP* violation and the limits of the standard model, p. 235, and Iowa State University Ames—AMES-HET-94-12.

[13] N. Cabibbo and A. Maksymowicz, Phys. Rev. **137**, B438 (1965); **168**, 1926(E) (1968).

[14] J. R. Dell'Aquila and C. A. Nelson, Phys. Rev. D **33**, 80 (1986); **33**, 93 (1986); C. A. Nelson, Phys. Rev. D **37**, 1220 (1988).

[15] T. Plehn, D. L. Rainwater, and D. Zeppenfeld, Phys. Rev. Lett. **88**, 051801 (2002); K. Hagiwara, Q. Li, and K. Mawatari, J. High Energy Phys. 07 (2009) 101; C. Englert, D. Goncalves, G. Nail, and M. Spannowsky, Phys. Rev. D **88**, 013016 (2013); K. Hagiwara and S. Mukhopadhyay, J. High Energy Phys. 05 (2013) 019; M. R. Buckley, T. Plehn, and M. J. Ramsey-Musolf, Phys. Rev. D **90**, 014046 (2014); arXiv:1403.2726; J. Brehmer, J. Jaeckel, and T. Plehn, Phys. Rev. D **90**, 054023 (2014); A. Greljo, G. Isidori, J. M. Lindert, and D. Marzocca, Eur. Phys. J. C **76**, 158 (2016).

[16] V. Hankele, G. Klamke, D. Zeppenfeld, and T. Figy, Phys. Rev. D **74**, 095001 (2006).

[17] N. Desai, D. K. Ghosh, and B. Mukhopadhyaya, Phys. Rev. D **83**, 113004 (2011); R. Godbole, D. J. Miller, K. Mohan, and C. D. White, Phys. Lett. B **730**, 275 (2014); C. Delaunay, G. Perez, H. de Sandes, and W. Skiba, Phys. Rev. D **89**, 035004 (2014); R. M. Godbole, D. J. Miller, K. A. Mohan, and C. D. White, J. High Energy Phys. 04 (2015) 103; S. Dwivedi, D. K. Ghosh, B. Mukhopadhyaya, and A. Shivaji, Phys. Rev. D **93**, 115039 (2016).

[18] S. Y. Choi, D. J. Miller, M. M. Muhlleitner, and P. M. Zerwas, Phys. Lett. B **553**, 61 (2003); R. M. Godbole, D. J. Miller, and M. M. Muhlleitner, J. High Energy Phys. 12 (2007) 031; C. Englert, C. Hackstein, and M. Spannowsky, Phys. Rev. D **82**, 114024 (2010); D. Stolarski and R. Vega-Morales, Phys. Rev. D **86**, 117504 (2012); I. Anderson *et al.*, Phys. Rev. D **89**, 035007 (2014); Y. Chen and R. Vega-Morales, J. High Energy Phys. 04 (2014) 057; N. Belyaev, R. Konoplich, L. E. Pedersen, and K. Prokofiev, Phys. Rev. D **91**, 115014 (2015).

[19] S. Bolognesi, Y. Gao, A. V. Gritsan, K. Melnikov, M. Schulze, N. V. Tran, and A. Whitbeck, Phys. Rev. D **86**, 095031 (2012).

[20] F. Bishara, Y. Grossman, R. Harnik, D. J. Robinson, J. Shu, and J. Zupan, J. High Energy Phys. 04 (2014) 084.

[21] C. Englert, K. Nordström, K. Sakurai, and M. Spannowsky, Phys. Rev. D **95**, 015018 (2017).

[22] C. Englert, D. Goncalves-Netto, K. Mawatari, and T. Plehn, J. High Energy Phys. 01 (2013) 148.

[23] M. J. Dolan, P. Harris, M. Jankowiak, and M. Spannowsky, Phys. Rev. D **90**, 073008 (2014).

[24] J. Ellis, D. S. Hwang, K. Sakurai, and M. Takeuchi, J. High Energy Phys. 04 (2014) 004; F. Demartin, F. Maltoni, K. Mawatari, B. Page, and M. Zaro, Eur. Phys. J. C **74**, 3065 (2014); S. Khatibi and M. Mohammadi Najafabadi, Phys. Rev. D **90**, 074014 (2014); F. Boudjema, R. M. Godbole, D. Guadagnoli, and K. A. Mohan, Phys. Rev. D **92**, 015019 (2015); K. Kolodziej and A. Slapik, Eur. Phys. J. C **75**, 475 (2015); M. R. Buckley and D. Goncalves, Phys. Rev. Lett. **116**, 091801 (2016).

[25] S. Berge, W. Bernreuther, and J. Ziethe, Phys. Rev. Lett. **100**, 171605 (2008); S. Berge, W. Bernreuther, B. Niepelt, and H. Spiesberger, Phys. Rev. D **84**, 116003 (2011); R. Harnik, A. Martin, T. Okui, R. Primulando, and F. Yu, Phys. Rev. D **88**, 076009 (2013); S. Berge, W. Bernreuther, and S. Kirchner, Phys. Rev. D **92**, 096012 (2015); T. Han, S. Mukhopadhyay, B. Mukhopadhyaya, and Y. Wu, J. High Energy Phys. 05 (2017) 128; E. Barberio, B. Le, E. Richter-Was, Z. Was, D. Zanzi, and J. Zaremba, Phys. Rev. D **96**, 073002 (2017).

[26] A. V. Manohar and M. B. Wise, Phys. Lett. B **636**, 107 (2006); A. Freitas and P. Schwaller, Phys. Rev. D **87**, 055014 (2013); J. Brod, U. Haisch, and J. Zupan, J. High Energy Phys. 11 (2013) 180; S. Dwivedi, D. K. Ghosh, B. Mukhopadhyaya, and A. Shivaji, Phys. Rev. D **92**, 095015 (2015); Y. T. Chien, V. Cirigliano, W. Dekens, J. de Vries, and E. Mereghetti, J. High Energy Phys. 02 (2016) 011; F. Ferreira, B. Fuks, V. Sanz, and D. Sengupta, arXiv:1612.01808.

[27] K. Kondo, J. Phys. Soc. Jpn. **57**, 4126 (1988); K. Kondo, J. Phys. Soc. Jpn. **60**, 836 (1991); R. H. Dalitz and G. R. Goldstein, Phys. Rev. D **45**, 1531 (1992); D. Atwood and A. Soni, Phys. Rev. D **45**, 2405 (1992); Y. Gao, A. V. Gritsan, Z. Guo, K. Melnikov, M. Schulze, and N. V. Tran, Phys. Rev. D **81**, 075022 (2010); A. V. Gritsan, R. Röntsch,

M. Schulze, and M. Xiao, Phys. Rev. D **94**, 055023 (2016); for some recent progress beyond leading order, see e.g. T. Martini and P. Uwer, J. High Energy Phys. 09 (2015) 083.
[28] For a review, see e.g. K. Cranmer, arXiv:1503.07622.
[29] J. Brehmer, K. Cranmer, F. Kling, and T. Plehn, Phys. Rev. D **95**, 073002 (2017).
[30] B. Efron, Ann. Stat. **3**, 1189 (1975); S. Amari, *Differential Theoretical Methods in Statistics* (Springer, New York, 1985).
[31] R. C. Rao, Bull. Calcutta Math. Soc. **37**, 81 (1945); H. Cramér, *Mathematical Methods of Statistics* (Princeton University Press, Princeton, NJ, 1946).
[32] K. Cranmer and T. Plehn, Eur. Phys. J. C **51**, 415 (2007).
[33] A. De Rujula, R. Petronzio, and B. E. Lautrup, Nucl. Phys. **B146**, 50 (1978); J. G. Korner, G. Kramer, G. Schierholz, K. Fabricius, and I. Schmitt, Phys. Lett. **94B**, 207 (1980); K. Hagiwara, K. i. Hikasa, and N. Kai, Phys. Rev. Lett. **52**, 1076 (1984); K. Hagiwara, T. Kuruma, and Y. Yamada, Nucl. Phys. **B369**, 171 (1992); A. Brandenburg, L. J. Dixon, and Y. Shadmi, Phys. Rev. D **53**, 1264 (1996); K. Hagiwara, K. i. Hikasa, and H. Yokoya, Phys. Rev. Lett. **97**, 221802 (2006); K. Hagiwara, K. Mawatari, and H. Yokoya, J. High Energy Phys. 12 (2007) 041; D. Choudhury and Mamta, Phys. Rev. D **74**, 115019 (2006).
[34] D. Atwood, S. Bar-Shalom, G. Eilam, and A. Soni, Phys. Rep. **347**, 1 (2001).
[35] A. M. Sirunyan *et al.* (CMS Collaboration), Phys. Lett. B **775**, 1 (2017).
[36] K. Hagiwara, S. Ishihara, R. Szalapski, and D. Zeppenfeld, Phys. Rev. D **48**, 2182 (1993); T. Corbett, O. J. P. Eboli, J. Gonzalez-Fraile, and M. C. Gonzalez-Garcia, Phys. Rev. D **87**, 015022 (2013).
[37] B. Grzadkowski, M. Iskrzynski, M. Misiak, and J. Rosiek, J. High Energy Phys. 10 (2010) 085.
[38] J. F. Gunion, H. E. Haber, G. L. Kane, and S. Dawson, Front. Phys. **80**, 1 (2000).
[39] M. Buschmann, C. Englert, D. Goncalves, T. Plehn, and M. Spannowsky, Phys. Rev. D **90**, 013010 (2014); E. Bagnaschi, R. V. Harlander, H. Mantler, A. Vicini, and M. Wiesemann, J. High Energy Phys. 01 (2016) 090; T. Neumann and C. Williams, Phys. Rev. D **95**, 014004 (2017); Phys. Rev. Lett. **118**, 252002 (2017).
[40] J. Campbell, M. Carena, R. Harnik, and Z. Liu, Phys. Rev. Lett. **119**, 181801 (2017); **119**, 199901(A) (2017).
[41] D. Rainwater, D. Zeppenfeld, and K. Hagiwara, Phys. Rev. D **59**, 014037 (1998); T. Plehn, D. L. Rainwater, and D. Zeppenfeld, Phys. Rev. D **61**, 093005 (2000).
[42] T. Plehn, P. Schichtel, and D. Wiegand, Phys. Rev. D **89**, 054002 (2014).
[43] F. Kling, T. Plehn, and P. Schichtel, Phys. Rev. D **95**, 035026 (2017).
[44] J. Alwall, R. Frederix, S. Frixione, V. Hirschi, F. Maltoni, O. Mattelaer, H.-S. Shao, T. Stelzer, P. Torrielli, and M. Zaro, J. High Energy Phys. 07 (2014) 079.
[45] R. Kleiss and W. J. Stirling, Phys. Lett. B **200**, 193 (1988); U. Baur and E. W. N. Glover, Phys. Lett. B **252**, 683 (1990); V. D. Barger, K. m. Cheung, T. Han, J. Ohnemus, and D. Zeppenfeld, Phys. Rev. D **44**, 1426 (1991); D. L. Rainwater, R. Szalapski, and D. Zeppenfeld, Phys. Rev. D **54**, 6680 (1996); B. E. Cox, J. R. Forshaw, and A. D. Pilkington, Phys. Lett. B **696**, 87 (2011); E. Gerwick, T. Plehn, and S. Schumann, Phys. Rev. Lett. **108**, 032003 (2012).
[46] D. Rainwater, arXiv:hep-ph/0702124; M. Rauch, arXiv: 1610.08420.
[47] J. Brehmer, A. Freitas, D. Lopez-Val, and T. Plehn, Phys. Rev. D **93**, 075014 (2016); A. Biekötter, J. Brehmer, and T. Plehn, Phys. Rev. D **94**, 055032 (2016).
[48] G. Aad *et al.* (ATLAS Collaboration), J. High Energy Phys. 04 (2015) 117.
[49] J. Brehmer, Ph.D. thesis, Heidelberg University, 2017, http://www.thphys.uni-heidelberg.de/plehn/includes/theses/brehmer_d.pdf.
[50] V. Khachatryan *et al.* (CMS Collaboration), J. Instrum. **10**, P02006 (2015).
[51] G. Isidori and M. Trott, J. High Energy Phys. 02 (2014) 082.